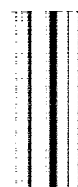# TECHNICAL REPORT R–94

SIMILARITY OF NEAR NOISE FIELDS OF SUBSONIC JETS

By WALTON L. HOWES

Lewis Research Center
Cleveland, Ohio

I

TECHNICAL REPORT R-94

SIMILARITY OF NEAR NOISE FIELDS OF SUBSONIC JETS

By WALTON L. HOWES

SUMMARY

Similarity relations for time-averaged fluctuating pressures at arbitrary field points are derived for subsonic jets. The derivation is based on elementary considerations for similarity in conjunction with known proportionality relations for the limiting cases of acoustic (compressible) fluctuations at points far from the flow and pressure fluctuations associated with incompressibility within the flow. The resulting relations are compatible with, and slightly more general than, previously proposed relations. Similarity relations are derived for overall pressure fluctuations as well as pressure fluctuations in frequency pass-bands of arbitrary width.

The derived relations were found to be sufficient, from an engineering standpoint, for predicting contour maps of overall and frequency-pass-band pressure fluctuations for intermediate values of the fluid and geometric variables if contour maps were available for two values of these variables. The derived relations could also be used in conjunction with test data for predicting spectra. However, in all instances geometric and dynamic similarity of the jets is essential. Dissimilarity of nozzle contours and differing jet temperatures seriously limit application of similarity relations, especially near the jet nozzle.

INTRODUCTION

Deleterious effects of high noise levels associated with jet propulsion devices have been widely publicized. In the search for methods of abating the noise at its source, knowledge of the noise characteristics is invariably required. General and simple specifications of these characteristics have utilized similarity parameters. When applicable, similarity parameters permit scaling, or prediction, of noise characteristics for a desired set of test conditions if the characteristics are known for a set of reference conditions.

The similarity of noise characteristics in the region remote from a jet (acoustic far field) has been fairly well established (refs. 1 to 7). Similarities of noise characteristics in the region near a jet (acoustic near field) are relatively undetermined. Theories and experiments concerned with the near field have usually dealt with two different quantities (acoustic power and pressure fluctuations, respectively) which are not simply related. The theories (refs. 4 and 8 to 10) are concerned primarily with the distribution of noise sources along a jet. Apparently the only attempt to determine similarity conditions throughout the near field was reported by Greatrex in reference 11.

In the present report near-field-similarity laws are discussed and tested using new, as well as previously reported (refs. 12 to 14), data. The results are restricted to jets issuing from nozzles having circular cross sections. The data are presented in a variety of forms for convenience in engineering applications.

SIMILARITY RELATIONS

When distances measured from a multipole noise source to points in the noise field are not large compared to a typical wavelength of the emitted sound, the field points are said to be located in the acoustic near field. If the source consists of an extended distribution of poles or multipoles, then field points which are not at large distances from the source compared to the extent of the source also are often considered to lie within the near field. Franz (ref. 15) has referred to the former region as the "induction near field" and to the latter region as the "geometric near field."

1

Noise fields associated with flow fields are hypothesized to be similar if the flow fields are geometrically and dynamically similar. Dynamical similarity is to be expected for all sufficiently large values of the overall flow Reynolds number UD/η and local Reynolds number Uz/η, where η is the kinematic viscosity of the fluid. However, in a jet, viscous forces may be of comparable magnitude to inertial and pressure forces very near the nozzle exit. Thus, dynamical similarity may not exist in this region; hence, similarity of the noise field should not be expected in the immediate vicinity. When similarity conditions are satisfied, noise characteristics should be uniquely describable nondimensionally in terms of a characteristic flow velocity, a characteristic length, and nondimensional space coordinates. Flow similarity is discussed in considerable detail in reference 16.

OVERALL PRESSURE FLUCTUATIONS

Greatrex effectively proposed (ref. 11) the following similarity relation: Given a round jet for which the space distribution of overall pressure fluctuations is known. Then, the space distribution of the overall pressure fluctuations for a second, similar, jet is given by

$$\overline{p_2^2}\left(\frac{D_2}{D_1}r_1,\theta_1\right) = (U_2/U_1)^n \overline{p_1^2}(r_1,\theta_1)$$

where p is the pressure fluctuation, U is the nozzle-exit velocity, D is the nozzle-exit diameter, and r and θ are spherical coordinates (fig. 1). (All
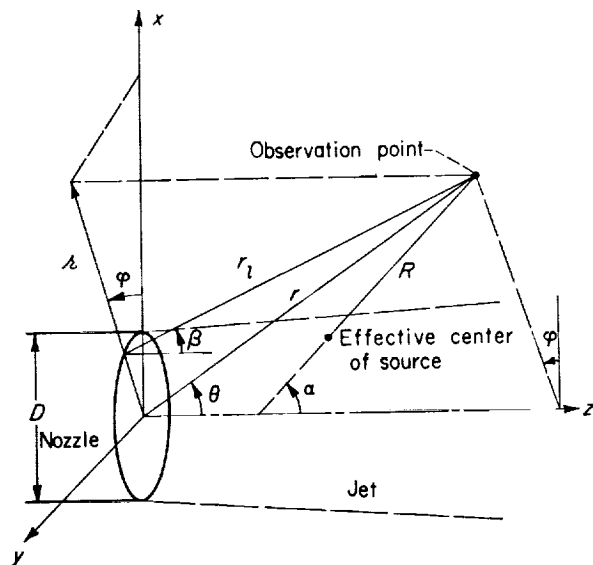

FIGURE 1.—Coordinate systems.

quantities are defined in the appendix.) (Note that for an axisymmetric jet, the noise field expressed in spherical coordinates is, effectively, independent of the azimuthal coordinate φ.) Subscript 1 refers to the jet for which the pressure field is known; subscript 2 refers to the jet for which the pressure field is to be determined. The exponent n is a function of the space coordinates and is to be determined from the characteristics of the noise field of the reference jet (denoted by the subscript 1) for two values of the velocity U. The preceding relation should apply for subsonic jets which are geometrically and dynamically similar.

In the experimental test (ref. 11) of Greatrex's proposed similarity condition, the noise levels of the unknown and reference jets at geometrically similar points generally differed by an amount (<2 db) not much greater than the errors of measurement. Thus, although the proposed relation appeared satisfactory for scaling results between jet engines of comparable size and thrust, the experiment could not be expected to test the validity of the proposed relation.

In determining, for overall pressure fluctuations, a similarity relation expected to apply throughout the noise field, consider the known proportionality relations between jet characteristics and pressure fluctuations. The far-field relation for acoustic pressure is

$$\overline{p^2}(r,\theta) \propto \rho^2 U^8 a^{-4} D^2 R^{-2} F_1(\alpha) \qquad (R \gg \lambda, D) \qquad (1)$$

(ref. 7) where ρ is the ambient density, a is the ambient speed of sound, R is a characteristic radius of the observation point from the effective center of the source, $F_1(\alpha)$ is a directivity function, and λ is a typical acoustic wavelength. In the far field, $R \to r$ and $\alpha \to \theta$. The limiting relation for pressure fluctuations in the near field is, in a form comparable to relation (1),

$$\overline{p^2}(r,\theta) \propto \rho^2 U^4 a^0 D^0 R^0 F_2(\alpha) \qquad (R \ll \lambda) \qquad (2)$$

(refs. 17 and 18). Considering the limiting relations (1) and (2), the following general relation is expected to apply at an arbitrary field point:

$$\overline{p^2}(r,\theta) \propto \rho^2 U^n a^{-m} D^l R^{-k} F(\alpha) \qquad (3a)$$

where n, m, l, and k are functions of the observation point. This may be rewritten as

$$\overline{p^2}(r,\theta) \propto \rho^2 U^4 (U/a)^m (R/D)^{-l} F(\alpha) \qquad (3b)$$

Proportionality (3b) results from the fact that $U^n a^{-m} D^l R^{-k}$ must possess the dimensions of (velocity)^4—so that $n=m+4$ (cf. relations (1) and (2))—and that D and R occur as a dimensionless ratio in relations (1) and (2). Proportionalities (3) apply to an individual jet.

Now, as before, consider two similar jets denoted by subscripts 1 and 2. At geometrically similar observation points, namely $(r_1/D_1,\theta_1) \sim (r_2/D_2,\theta_2)$, it follows that $R_1/D_1 = R_2/D_2$ and $\alpha_1 = \alpha_2$. Thus,

$$\overline{p_2^2}(r^*,\theta^*) = (\rho_2/\rho_1)^2 (U_2/U_1)^4 (U_2/a_2)^m (U_1/a_1)^{-m} \overline{p_1^2}(r^*,\theta^*)$$

where $r^* = r_1/D_1 = r_2/D_2$ and $\theta^* = \theta_1 = \theta_2$. This corresponds to a proportionality relation

$$\overline{p^2}(r^*,\theta^*)/\rho^2 U^4 \propto (U/a)^m \tag{4}$$

where m, a continuous function of the coordinates r^*,θ^*, possesses the values 0 and 4 at near-field and far-field limits, respectively, and may possess any value in the intermediate field. Relation (4) is compatible with Greatrex's proposal if ambient conditions remain unchanged.

PRESSURE FLUCTUATIONS IN FREQUENCY BANDS

For similarity of the space distribution of pressure fluctuations in frequency bands, Greatrex proposed (ref. 11) the use of the overall-pressure-similarity condition in the manner already described but with the additional stipulation that to be comparable the noise fields should be associated with frequency bands for which the Strouhal number fD/U is the same. No specification was placed on the frequency bandwidth for which the maps were to be defined. The method was illustrated using octave-band data.

To obtain a similarity relation which applies for frequency bands and is expected to apply throughout the noise field, define the mean-square-pressure spectral density $\overline{\psi^2}(f)$ as $\overline{p^2} = \int_0^\infty \overline{\psi^2}(f)\, df$, where f is the frequency. Considering proportionalities (1) and (2),

$$\overline{\psi^2}(r,\theta;f) \propto \rho^2 U^8 a^{-4} D^2 R^{-2} \hat{f}^{-1} G_1(\alpha;f) \qquad (R \gg \lambda, D) \tag{5}$$

$$\overline{\psi^2}(r,\theta;f) \propto \rho^2 U^4 a^0 D^0 R^0 \hat{f}^{-1} G_2(\alpha;f) \qquad (R \ll \lambda) \tag{6}$$

where $\hat{f} \propto U/D$ is a characteristic frequency associated with the overall flow. The directivity

functions G_1 and G_2 depend, also, on the frequency f. It follows from proportionalities (5) and (6) that, in general,

$$\overline{\psi^2}(r,\theta;f) \propto \rho^2 U^\nu a^{-\mu} D^\lambda R^{-\kappa} G(\alpha;f) \tag{7a}$$

which may be rewritten in the form

$$\overline{\psi^2}(r,\theta;f) \propto \rho^2 U^3 (U/a)^\mu (R/D)^{-\kappa} DG(\alpha;f) \tag{7b}$$

Relation (7b) results because $U^\nu a^{-\mu} D^\lambda R^{-\kappa}$ must possess the dimensions (velocity)^4 · time = (velocity)^3 · length, so that $\nu = \mu + 3$ and $\lambda = 1 + \kappa$. Proportionalities (7) apply to an individual jet.

For similar jets, values of $\overline{\psi^2}$ are to be compared for similar points (r^*,θ^*) and for similar frequencies $\nu = fD/U$. Thus,

$$\overline{\psi_2^2}(r^*,\theta^*;\nu) = (\rho_2/\rho_1)^2 (U_2/U_1)^3$$

$$(U_2/a_2)^\mu (U_1/a_1)^{-\mu} (D_2/D_1)\, \overline{\psi_1^2}(r^*,\theta^*;\nu)$$

which corresponds to a proportionality relation

$$\overline{\psi^2}(r^*,\theta^*;\nu)/\rho^2 U^3 D \propto (U/a)^\mu \tag{8}$$

where μ is a function of frequency, as well as the observation point.

Relation (8) applies to spectral densities. However, Greatrex considered comparisons for octave, rather than unit, bandwidths. By definition, for arbitrary bandwidth,

$$\overline{p^2}(r,\theta;f_a,f_b) = \int_{f_a}^{f_b} \overline{\psi^2}(r,\theta;f)\, df \tag{9}$$

where f_a and f_b are lower and upper cutoff frequencies, respectively. Thus, for similarity in frequency pass-bands,

$$\overline{p^2}(r^*,\theta^*;\nu_a,\nu_b) = \int_{\nu_a}^{\nu_b} \frac{U}{D} \overline{\psi^2}(r^*,\theta^*;\nu)\, d\nu \tag{10}$$

that is, the comparison must be made at geometrically similar field points (r^*,θ^*), and the Strouhal numbers corresponding to the cutoff frequencies must be identical. This latter requirement is expressed by $(\nu_a)_1 = (\nu_a)_2$ and $(\nu_b)_1 = (\nu_b)_2$. Equation (10) applies to overall pressure fluctuations, as well as to pressure fluctuations in pass-bands. In the former instance $\overline{p^2}(r^*,\theta^*;\nu_a,\nu_b)$ compares with $\overline{p^2}(r^*,\theta^*)$ if the pass-band contains the dominant portion of the entire spectrum.

A convenient dimensionless form for the spectrum follows from equation (10), namely,

$$\frac{\overline{p^2}\,(r^*,\theta^*;\nu_a,\nu_b)}{\overline{p^2}\,(r^*,\theta^*)}=\int_{\nu_a}^{\nu_b}\frac{U}{D}\frac{\overline{\psi^2}\,(r^*,\theta^*;\nu)}{\overline{p^2}\,(r^*,\theta^*)}\,d\nu \quad (11)$$

The left side of equation (11) represents a dimensionless form for the pressure fluctuations in pass-bands. The integrand in equation (11) represents a dimensionless form for the mean-square-pressure spectral density. Because $\overline{p^2}(r^*,$

(a) Photograph.

FIGURE 2.— Air-jet installation.

$\theta^*;\nu_a,\nu_b)$ possesses the dimensions of mean-square pressure, an alternative dimensionless form is

$$\overline{p^2}\,(r^*,\theta^*;\nu_a,\nu_b)/\rho^2U^4 \propto (U/a)^\mu \quad (12)$$

which expresses the same functional dependence as equation (4).

FLUCTUATION-PRESSURE SPECTRA

The preceding discussion applies, also, to spectra. Dimensionless spectral densities or dimensionless band-pass spectra for geometrically similar field points are to be compared for identical values of Strouhal number.

EXPERIMENT

APPARATUS

Air-jet facility.—The facility (fig. 2) is identical to that described in reference 7. Essentially, a continuous horizontal air jet is obtained at near-ambient temperature at a height 10 feet above the ground plane and more than 100 feet from the nearest structure other than the facility itself. The tank face was covered with a 4-inch-thick layer of acoustic absorbent material and the nozzle-inlet pipe with a 2-inch-thick layer of the same material in order to minimize reflections (cf. fig. 3).

Two nozzles (fig. 4), one having an exit diameter of 3 inches, the other of 5 inches, were used in the tests.

(b)

(b) Plan view (not to scale).
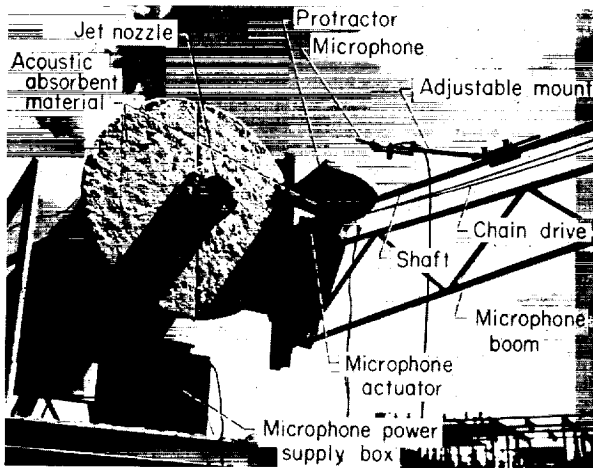
FIGURE 2.—Concluded. Air-jet installation.

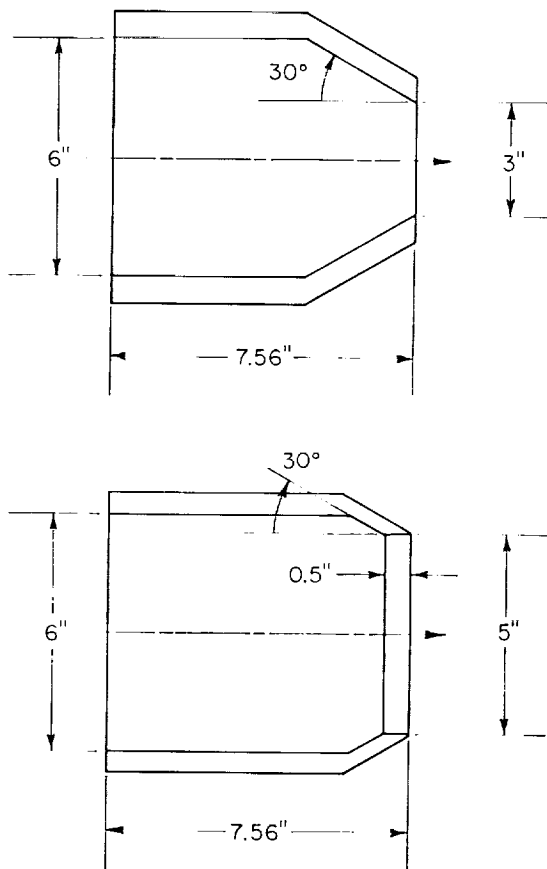FIGURE 3.—Jet nozzle and actuator mounting.

FIGURE 4.—Air-jet nozzle configurations.

Air pressures and temperatures were measured using manometers and thermocouples, respectively, in the same manner as described in reference 7 and at the points shown in figure 2(b).
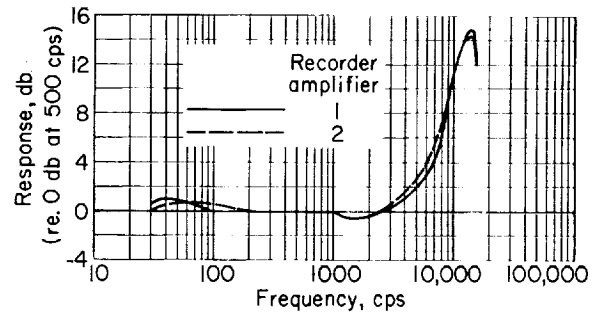

FIGURE 5.—Acoustic system frequency response (microphone input through tape playback). Record level—15 voice units; tape speed, 15 inches per second.

Acoustic recording.—The pressure transducer consisted of a commercial condenser microphone having a diaphragm approximately 7/16 inch in diameter and designed for operation at high acoustic pressures. The acoustic system was adapted (cf. ref. 7) for use with long cables and magnetic-tape recording. The system-frequency-response curve (from microphone input through playback) is shown in figure 5.

While recording noise, the microphone was moved linearly and continuously by an actuator driven by a synchronous motor. The rate of motion was constant (0.277 in./sec) over the traverse length (94.0 in.). The entire unit (fig. 3) was rotatable about a fixed vertical axis adjacent to the jet nozzle, permitting microphone traverses at any azimuth from 0° (parallel to the jet axis) to 100°. The angle of traverse was read from a protractor having a radius of 18 inches. A block diagram of the recording and actuation systems is shown in figure 6. Separate or simultaneous starting or stopping of the microphone motion and recording process was provided for. Reversal and automatic cessation of the motion were accomplished by limit switches actuated by the microphone holder.

The microphone was mounted in the horizontal plane containing the jet axis and pointed at and normal to the jet axis. The estimated probable error of the microphone position for any given traverse was $\left(\begin{smallmatrix}+0.1\\-0.3\end{smallmatrix}\right)$ inch in the vertical direction and ±0.1 inch in the horizontal plane. Hysteresis of the traverse was negligible.

Acoustic analysis.—Data were transcribed from the magnetic recordings by means of a one-third-octave band audiospectrum analyzer and automatic level-recorder.
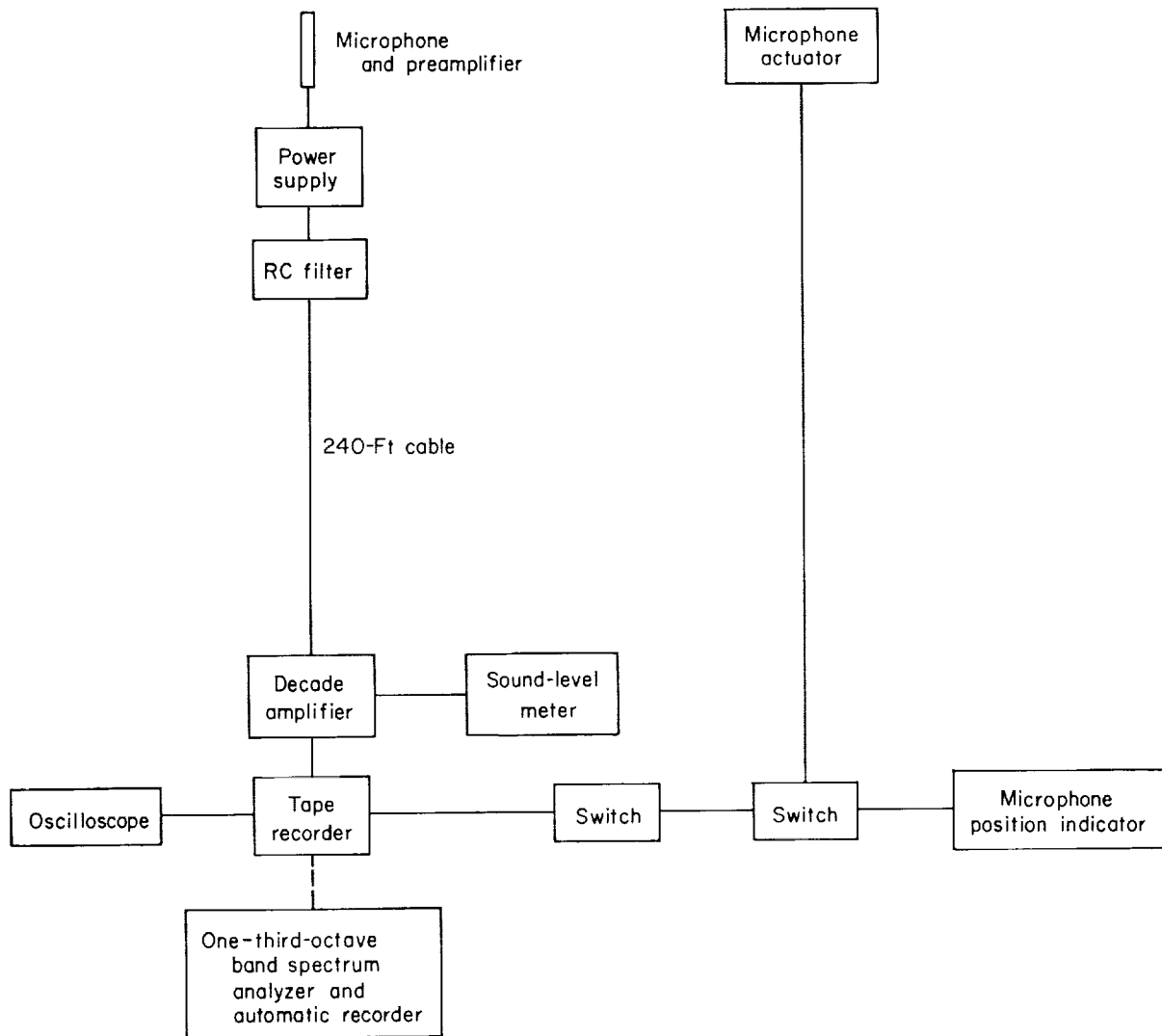
FIGURE 6.—Acoustic recording and microphone actuation systems.

PROCEDURE

Acoustic recording.—First the microphone boom was set at a predetermined angle θ. The microphone was then positioned within a fraction of an inch of the nozzle exit. The desired airflow conditions were established and the sound-level-meter reading noted. Microphone motion and acoustic recording were started simultaneously. Following completion of the microphone traverse, new flow conditions were established, and a new recording was made with the microphone moving toward the nozzle. At the end of the traverse the new sound level was noted. The entire process was repeated for several flow conditions and then for several traverse angles (10°, 15°, 30°, 45°, 60°, 75°, 90°, 100°). Impingement of the jet on the microphone prohibited traverses at angles less than 10°.

Preceding and following each series of recordings at a selected angle, the acoustic system was calibrated using an acoustic signal of known level (121 db re. 2×10^{-4} dyne/cm^2 at 400 cps at the microphone). The calibration signal was monitored using the sound-level meter. The monitored level was used to calculate the actual jet-noise level from the noise level noted when the microphone was adjacent to the nozzle exit in the presence of jet flow. Because of the continuity of the noise recordings, noise levels could then be readily determined throughout the traverse.

The insertion of a decade amplifier in the electronic circuit permitted the recorded signal level to be kept within the range of linear amplitude response of the magnetic tape. When necessary the amplification was switched during the recording process. Correction for the switching was made in reading the printed records.

Acoustic analysis.—The recordings obtained were converted to printed form using the analyzer-recorder. The printed records were used to obtain contour maps of the noise fields, as well as other graphical results. Although the automatic recorder had a quasi-peak characteristic, the starting noise levels were originally noted from a sound-level meter having a full-wave rectifying characteristic. During playback the noise signal was monitored using a root-mean-square voltmeter in addition to the sound-level meter. The difference between the sound levels indicated by the two instruments was always less than 1 decibel, but usually less than 0.5 decibel when both instruments were calibrated to yield the same level for a 1000-cycle-per-second sine-wave input.

The starting noise levels (at the nozzle exit) were found to vary for a single flow condition The standard deviation of the starting noise evel for an individual traverse angle with respect to the average level for a single flow condition (all angles) was 1 decibel, or less. In plotting contour maps the average recorded noise level at the nozzle exit was adopted as the starting level for each traverse.

Local pressure spectra were determined by replaying the same portion of the magnetic-tape-recorded signal through each filter of the spectrum analyzer. Thus, the indicated spectrum levels for all frequencies are simultaneous values, rather than consecutive values.

RESULTS AND DISCUSSION

The Reynolds number (UD/η) range associated with the 5-inch-diameter-nozzle results was 2.0×10^6 to 3.5×10^6, whereas the corresponding range for the 3-inch-diameter-nozzle results was 1.4×10^6 to 2.1×10^6. Although the mean-flow Reynolds number was not constant, studies of far noise fields (ref. 7) over the same range of values of Reynolds number have indicated that

similarity of jet noise fields is independent of Reynolds number over the present range of interest. Moreover, no effect of Reynolds number on similarity is to be expected unless the Reynolds number is small (say $<10^2$). The local Reynolds number (Uz/ν) is small near the nozzle exit. Thus, a Reynolds number effect may be associated with pressure fluctuations originating near the nozzle.

OVERALL-PRESSURE FLUCTUATIONS

Field-contour maps of overall-pressure fluctuations surrounding subsonic jets are shown in figures 7 and 8. The contours shown are those of overall-sound-pressure level $SPL=20 \log (\sqrt{\overline{p^2}}/p_0)$, where $p_0=2\times10^{-4}$ dyne/cm². Maps corresponding to the 3-inch-diameter nozzle are exhibited in figure 7, whereas those in figure 8 correspond to the 5-inch-diameter nozzle. In both cases maps corresponding to the limits of the measured subsonic-velocity range are included. The maps for a given nozzle exhibit evidence of a transition of the contour shapes as a function of jet velocity.

In order to predict the noise field for a jet, the distribution of the velocity exponent n (or $m=n-4$) must be determined from measurements of the noise fields associated with a reference jet for two values of the jet velocity. The distributions of n were calculated using the formula $n(r^*, \theta^*)=\dfrac{SPL''(r^*, \theta^*)-SPL'(r^*, \theta^*)}{10 \log (U''/U')}$, where the primes refer to the appropriate reference. Data illustrated in figures 7(a) and (c) were used in computing the distribution of n associated with the 3-inch-diameter nozzle, whereas data illustrated in figures 8(a) and (c) were used in computing n for the 5-inch-diameter nozzle. The results are shown in figure 9. The distribution of n for a turbojet engine (ref. 14) is shown in figure 10.

The distributions appearing in figure 9 have been smoothed considerably. From estimates of the errors in determining $SPL''-SPL'$, the estimated probable error of n was $\delta n \approx 1$, independent of n. This corresponds to a percentage error ranging from 10 to 25 (approx.). The magnitude of this error seems insufficient to account for the considerable difference among the three distributions of n.
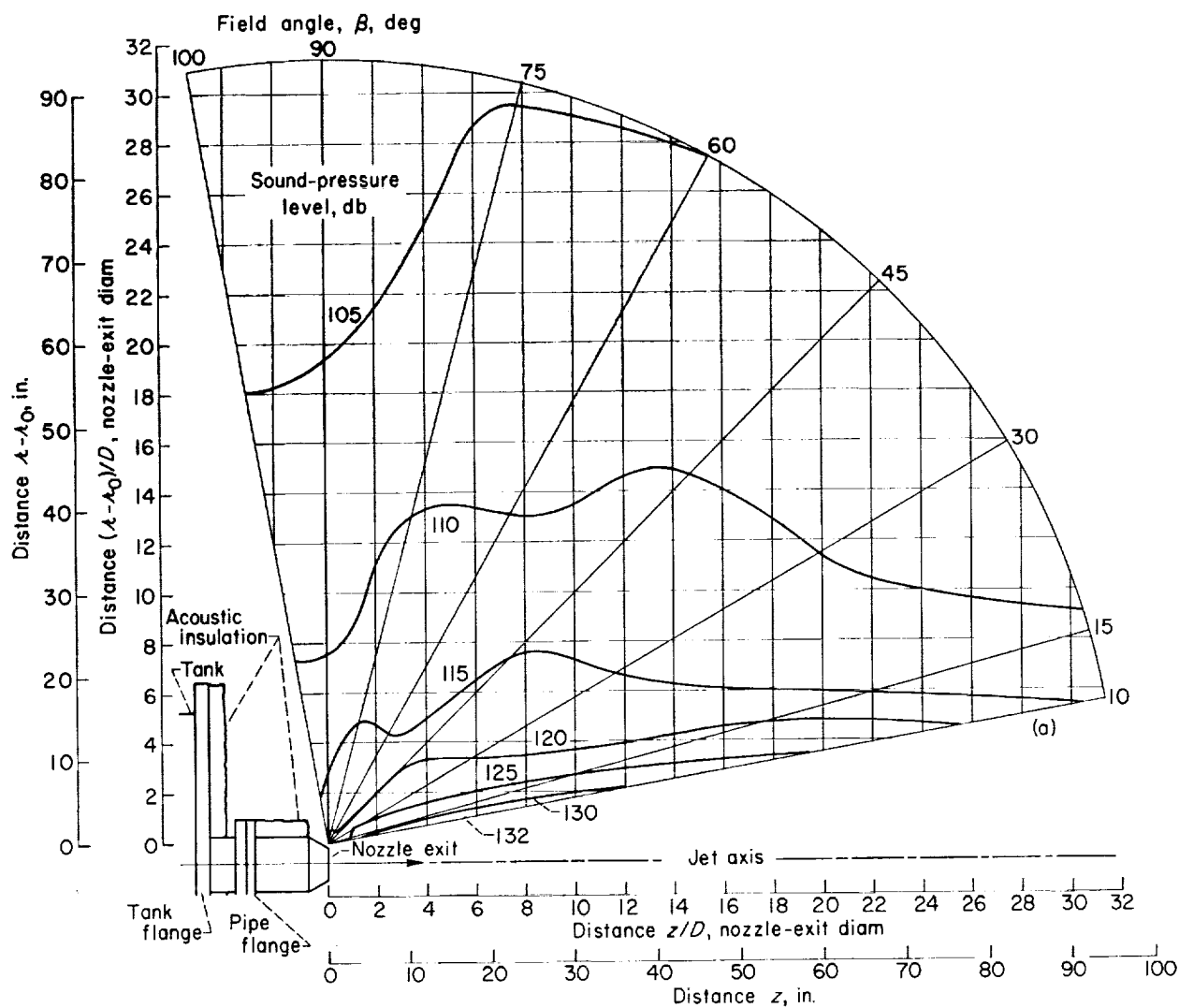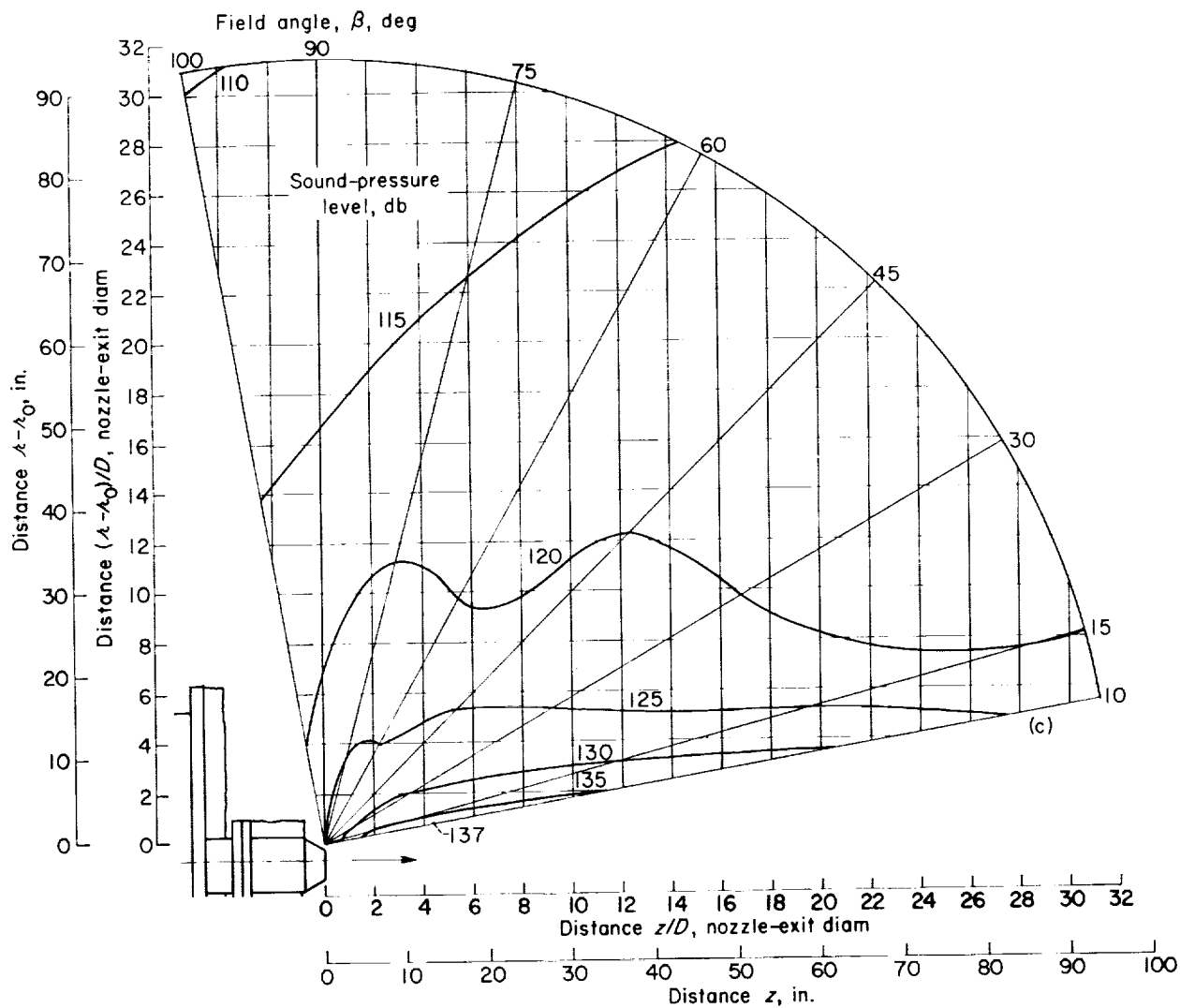
(a) Velocity U, 803 feet per second.

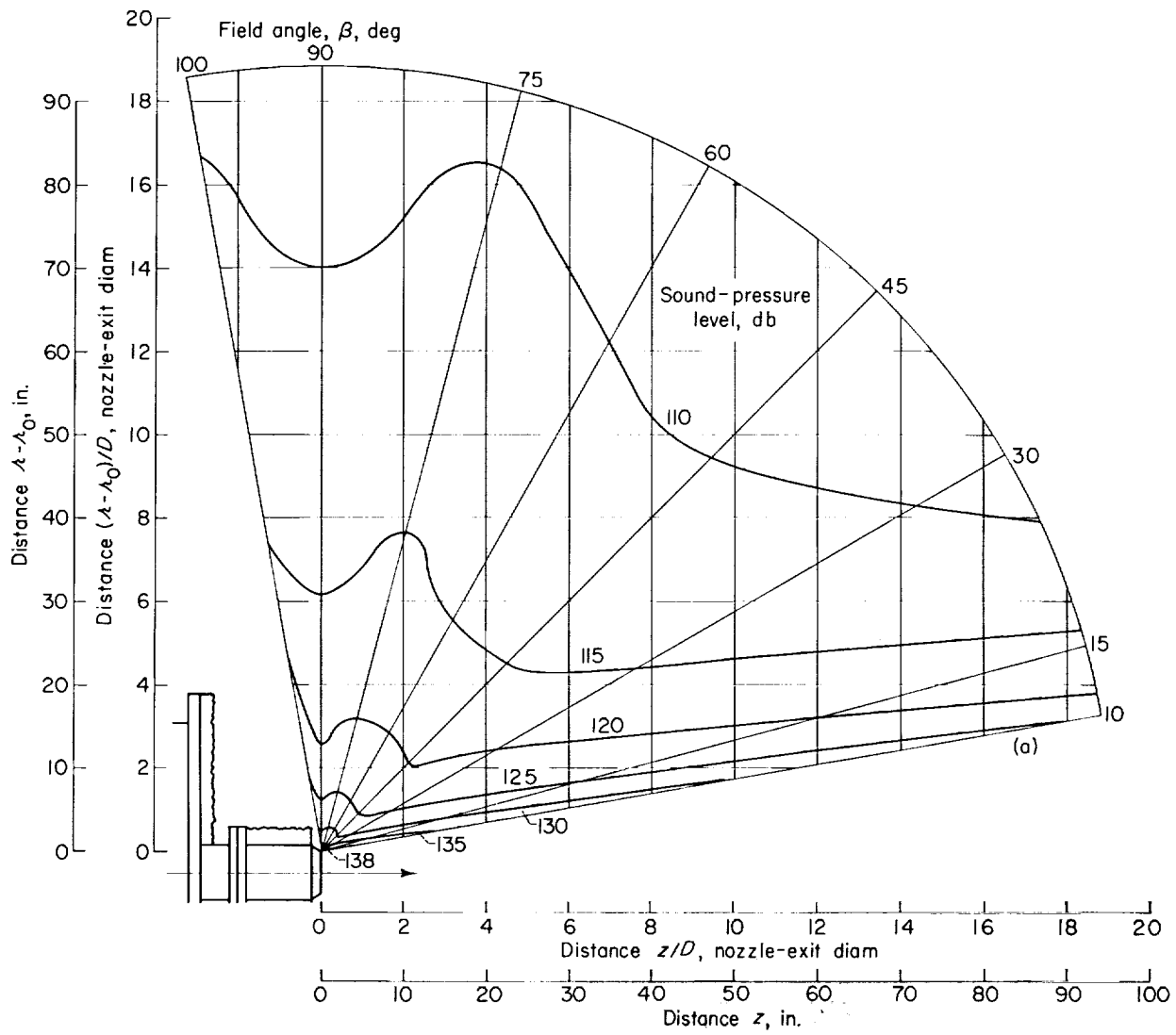FIGURE 7.—Contours of overall-sound-pressure level for a subsonic jet. Nozzle diameter D, 3 inches.
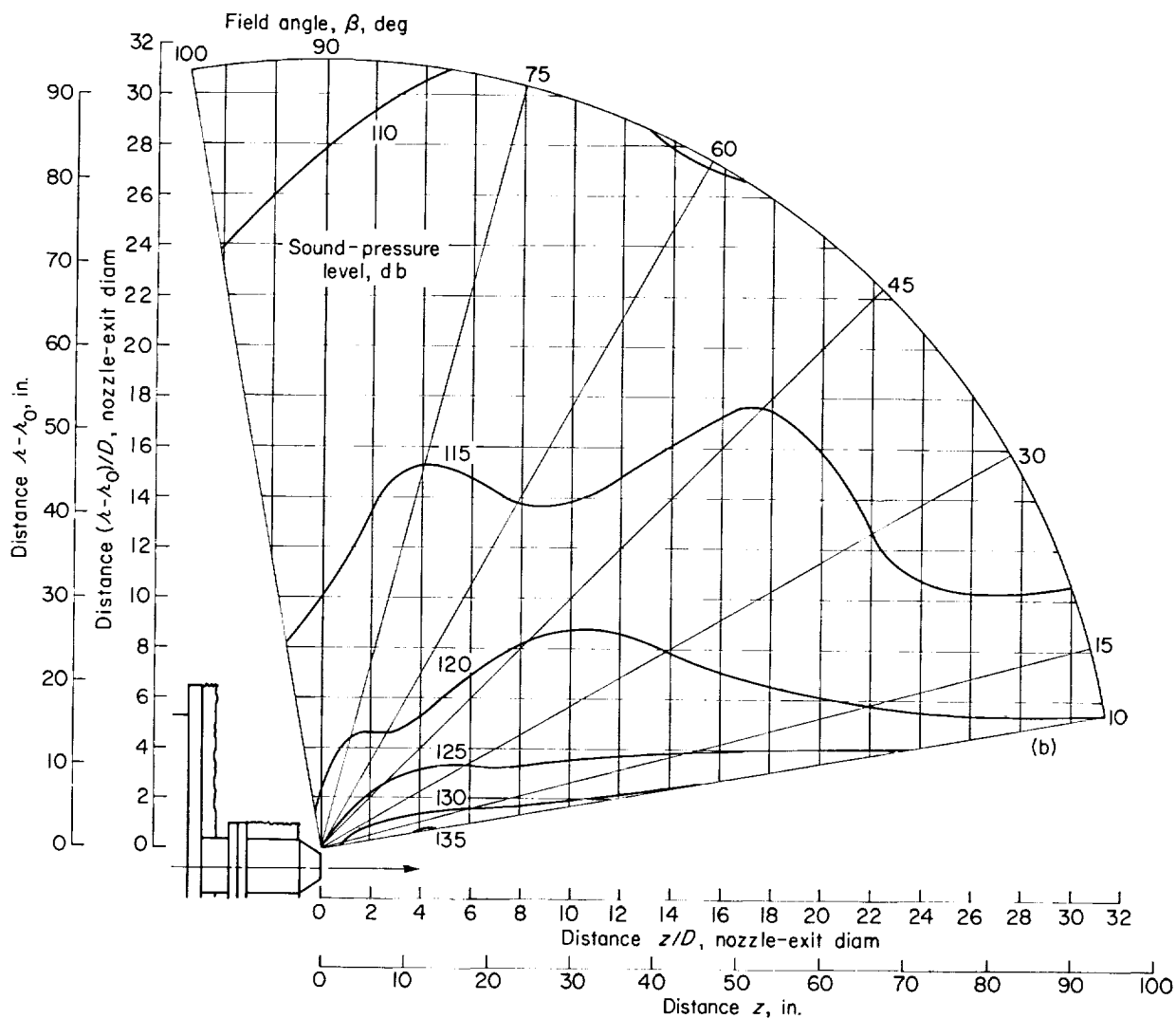
(b) Velocity U, 931 feet per second.

FIGURE 7.—Continued. Contours of overall-sound-pressure level for a subsonic jet. Nozzle diameter D, 3 inches.
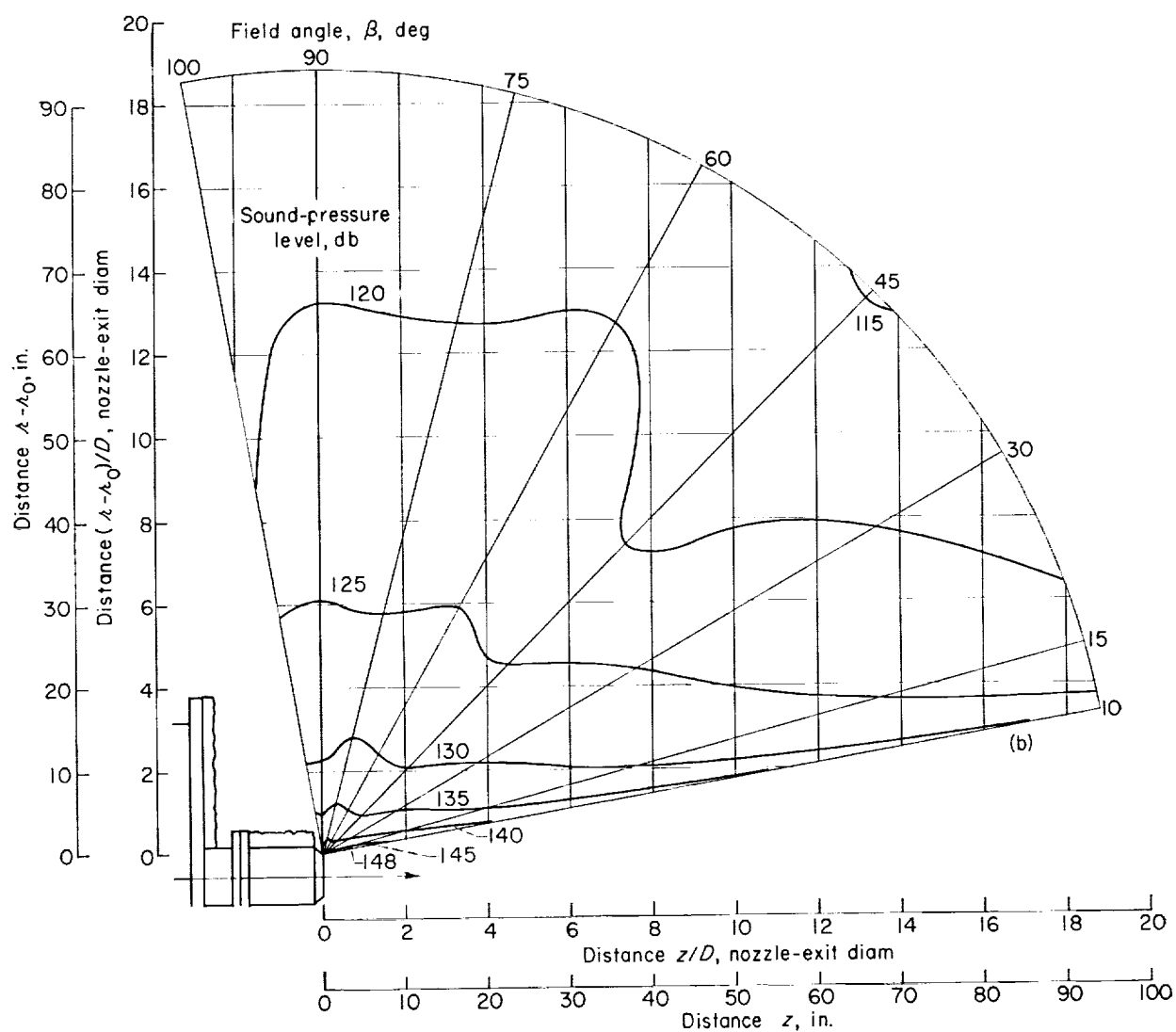
(c) Velocity U, 1021 feet per second.

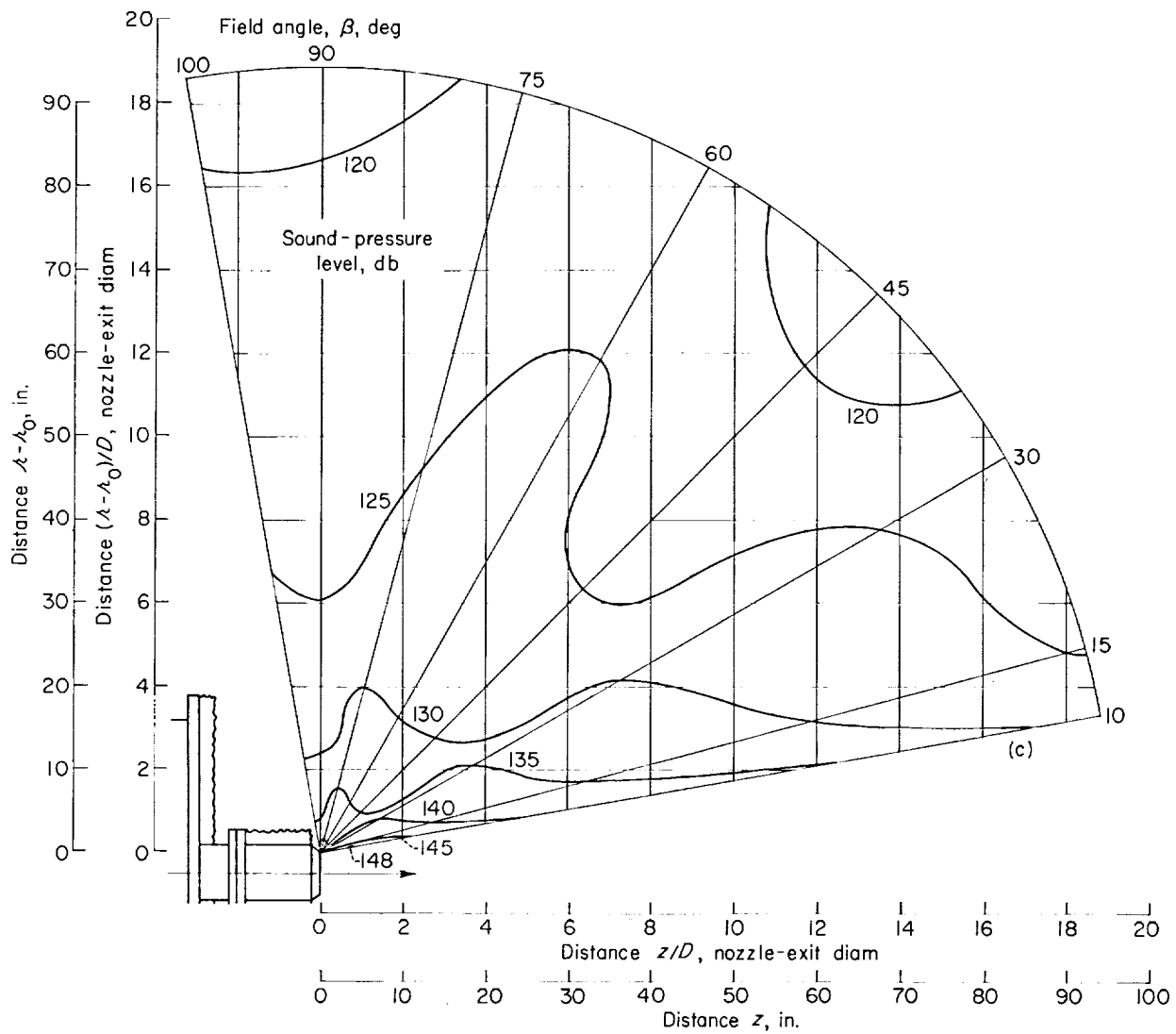FIGURE 7.—Concluded.   Contours of overall-sound-pressure level for a subsonic jet.   Nozzle diameter D, 3 inches.

(a) Velocity U, 690 feet per second.

FIGURE 8.—Contours of overall-sound-pressure level for a subsonic jet. Nozzle diameter D, 5 inches.

(b) Velocity U, 894 feet per second.

FIGURE 8.—Continued.   Contours of overall-sound-pressure level for a subsonic jet.   Nozzle diameter D, 5 inches.

(c) Velocity U, 1028 feet per second.

FIGURE 8.—Concluded. Contours of overall-sound-pressure level for a subsonic jet. Nozzle diameter D, 5 inches.
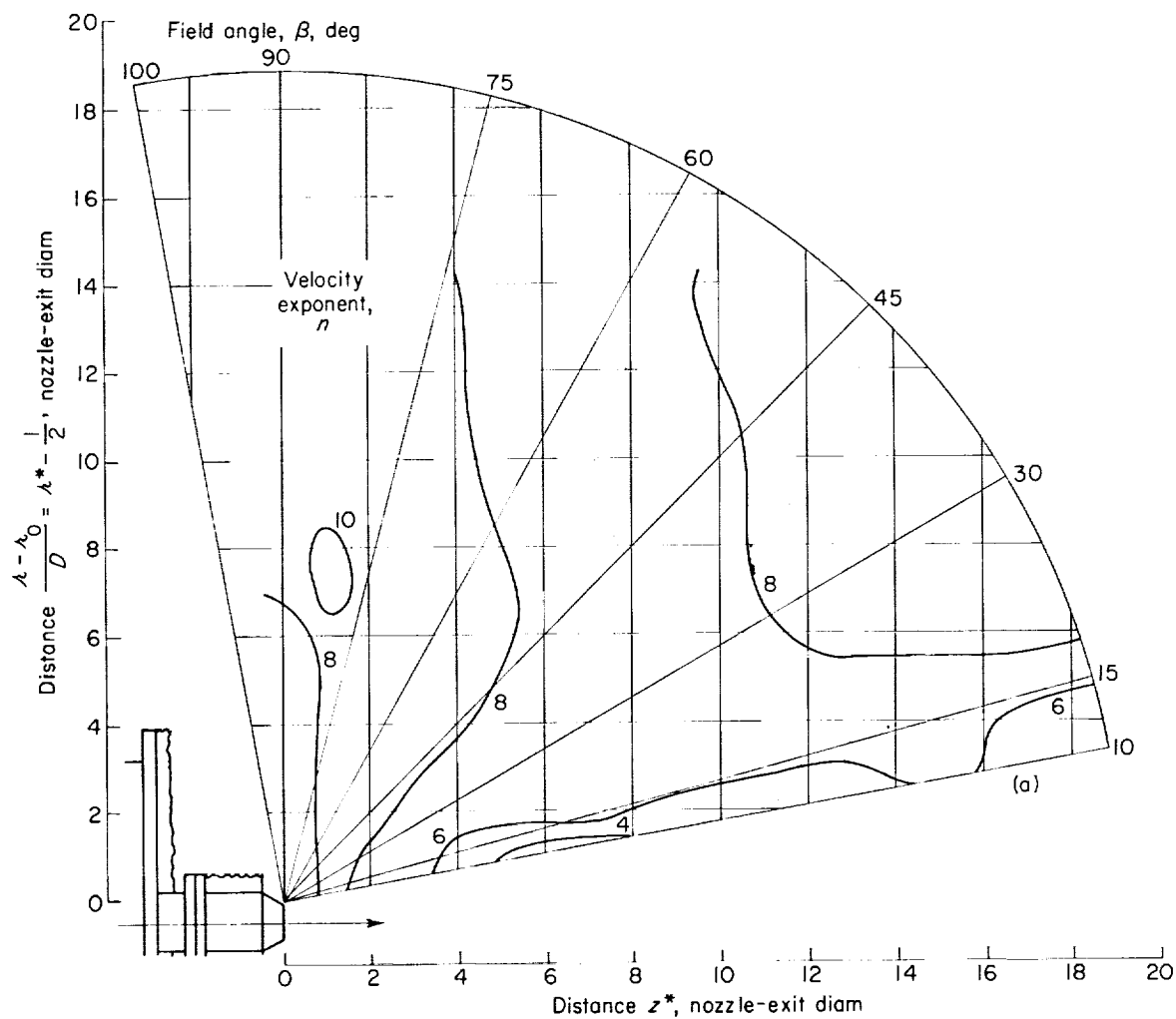
(a) 3-Inch-diameter nozzle.

FIGURE 9.—Distribution of velocity exponent n.
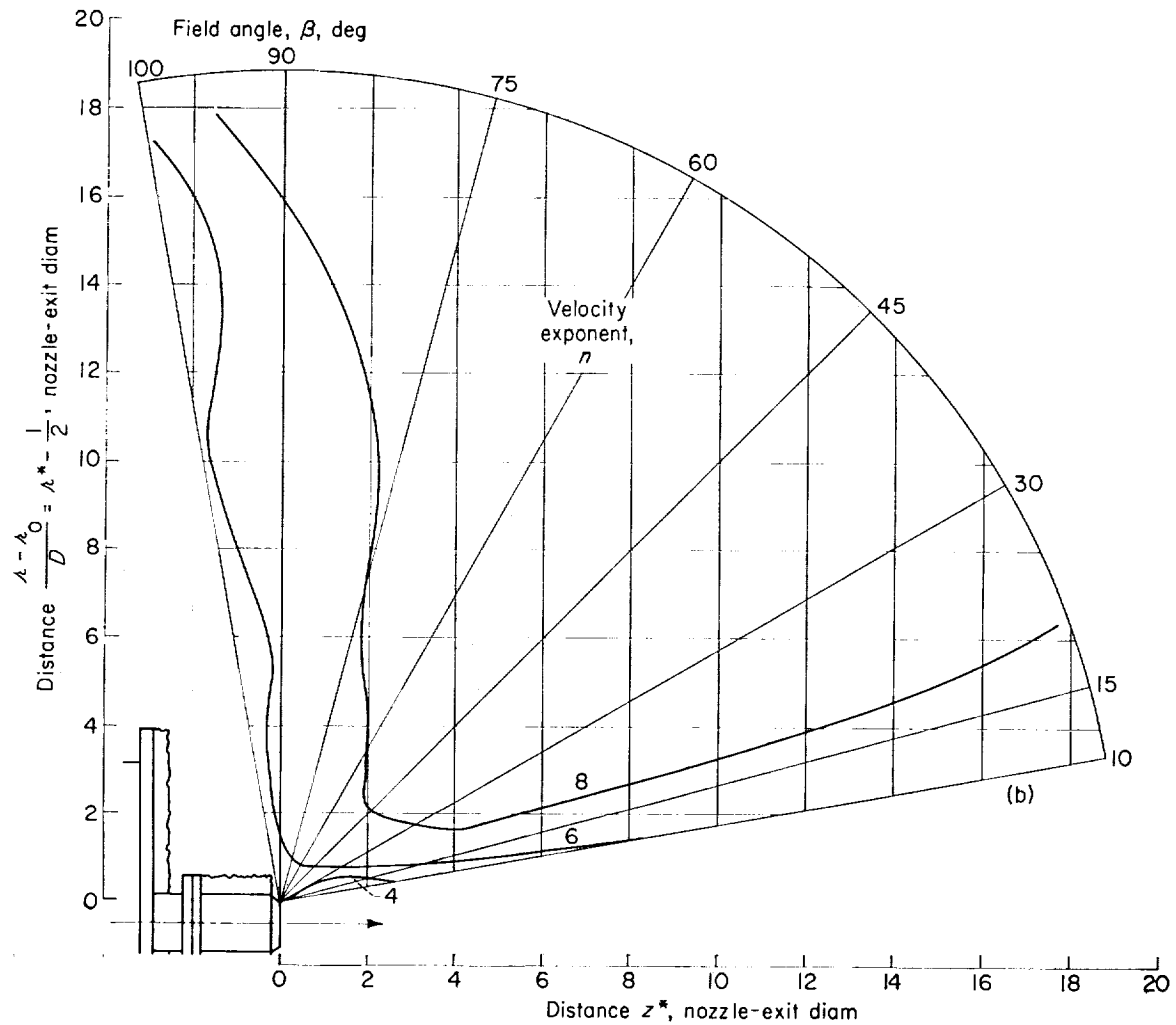
(b) 5-Inch-diameter nozzle.

FIGURE 9.—Concluded.   Distribution of velocity exponent *n.*
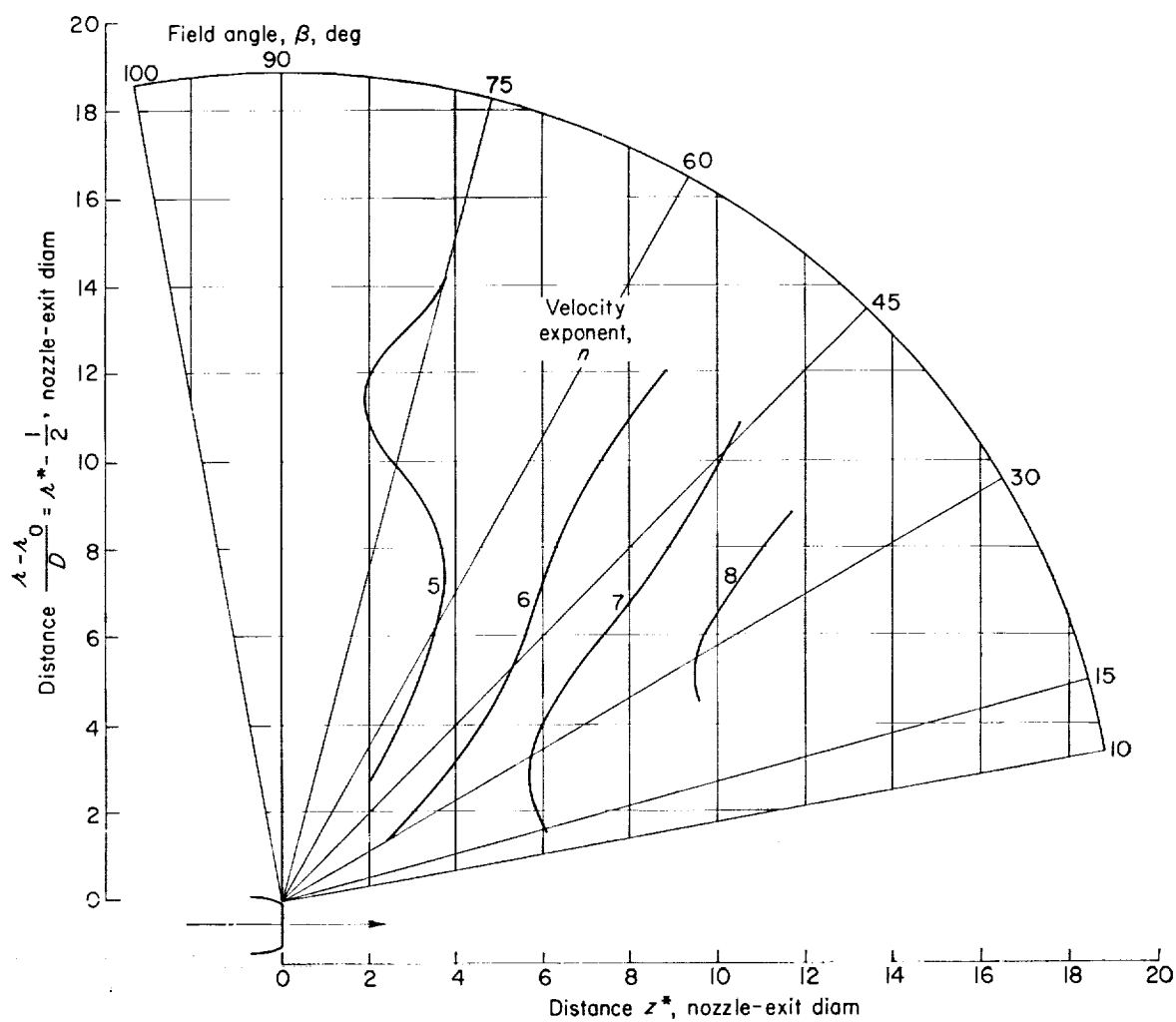
FIGURE 10.—Distribution of velocity exponent n for a turbojet engine (fig. 31 of ref. 14).

The distributions of n were used to predict contour maps associated with the two nozzles for values of jet velocity intermediate between the limiting reference values using the relation $SPL(r^*, \theta^*) = SPL'(r^*, \theta^*) + 10n(r^*, \theta^*) \log (U/U')$. In order to permit an experimental check of the predictions the velocities U were selected to correspond to the maps shown in figures 7(b) and 8(b). Comparisons between the predicted and experimentally determined maps are shown in figure 11. The predicted noise levels agree quite well with the measured levels at corresponding points. The difference of the levels is, at most, 2 or 3 decibels. This level difference at a point, not the spatial separation of the corresponding contour lines, is the appropriate measure of the error of the prediction. The difference between the measured and predicted levels at corresponding points was found to be approximately 1 decibel for every 5-decibel adjustment of the reference level to the predicted level.

Attempts to predict noise fields associated with the 5-inch-diameter nozzle and a turbojet engine, using 3-inch-diameter-nozzle data as the reference, failed. Disagreements between predicted and test results of the order of 10 decibels were obtained. The shapes of the convergent sections of the nozzles, that is, the nozzle contours, hence the jet structures, were not similar. These results imply that near noise fields of geometrically similar jets are similar over a fairly wide range of subsonic velocities, but that the degree of similarity is strongly influenced by changes of the jet nozzle contour (geometrical dissimilarity) (cf. ref. 12). In addition the turbojet engine exhaust was hot, whereas the air jets were cold. The jet temperature is also likely to affect similarity, that is, hot and cold jets cannot be expected to compare favorably on the present similarity basis (cf. ref. 12).

The distribution of time-averaged fluctuation pressures along the jet boundary is of particular interest because of its proximity to the noise sources. Dimensionless profiles of mean-square pressures along the mean-velocity boundary are shown for the various nozzles in figure 12. Predicted curves (cf. ref. 12) are also shown. In reference 12 the profiles shown are discussed in some detail. There, as herein, the differences between the predicted and measured pressure profiles are attributed to differences among the nozzle contours or differences between jet and

ambient temperatures. The magnitude of the difference between the pressure profiles associated with the 3- and 5-inch-diameter nozzles is so large (≈ 10 db near the nozzle) that an observable difference might be expected in the far field. The difference was observed (fig. 7 of ref. 7). The total acoustic power emitted by the jet associated with the 5-inch-diameter nozzle for all values of the Lighthill parameter $L = \rho D^2 U^8 a^{-5}$ was approximately 2 decibels higher than that associated with the 3-inch-diameter nozzle. This result could not be attributed to any difference between experimental conditions other than the nozzle contours.

The extent to which the nozzle contour would influence the near noise field was not fully appreciated when the tests were performed (although cf. ref. 16, p. 184 footnote). Thus, similarity of the noise field as a function of jet velocity was confirmed, but similarity associated with jet size could not be studied using the available nozzles. In addition, the effects of changing ambient conditions were not studied.

PRESSURE FLUCTUATIONS IN FREQUENCY BANDS

Contour maps of sound-pressure levels for one-third-octave bandwidths are shown in figures 13 and 14. Results for a relatively large value ($\nu_m \approx 5$, fig. 13) and a relatively small value ($\nu_m \approx 0.06$, fig. 14) of Strouhal number are presented. The similarity of the contour shapes for constant values of Strouhal number is evident. As expected, the apparent source of the pressure fluctuations for the larger value of ν_m is relatively near the nozzle exit, whereas the apparent source for the smaller value of ν_m is well downstream of the nozzle exit.

Contour maps of the mean-square-pressure-spectral-density level in the dimensionless form of the logarithm of $\dfrac{U}{D} \dfrac{\overline{\psi^2}(f)}{\overline{p^2}}$ (eq. (11)) are presented in figure 15. Each map was determined by averaging two similar contour maps for different values of the jet velocity. The contours indicate the relative contribution of the spectral density at the frequency f to the overall mean-square pressure. Thus, these maps indicate that the relative contribution of the low frequencies to the mean-square pressure is greatest near the jet boundary, whereas the greatest relative contribution of the high frequencies occurs at a
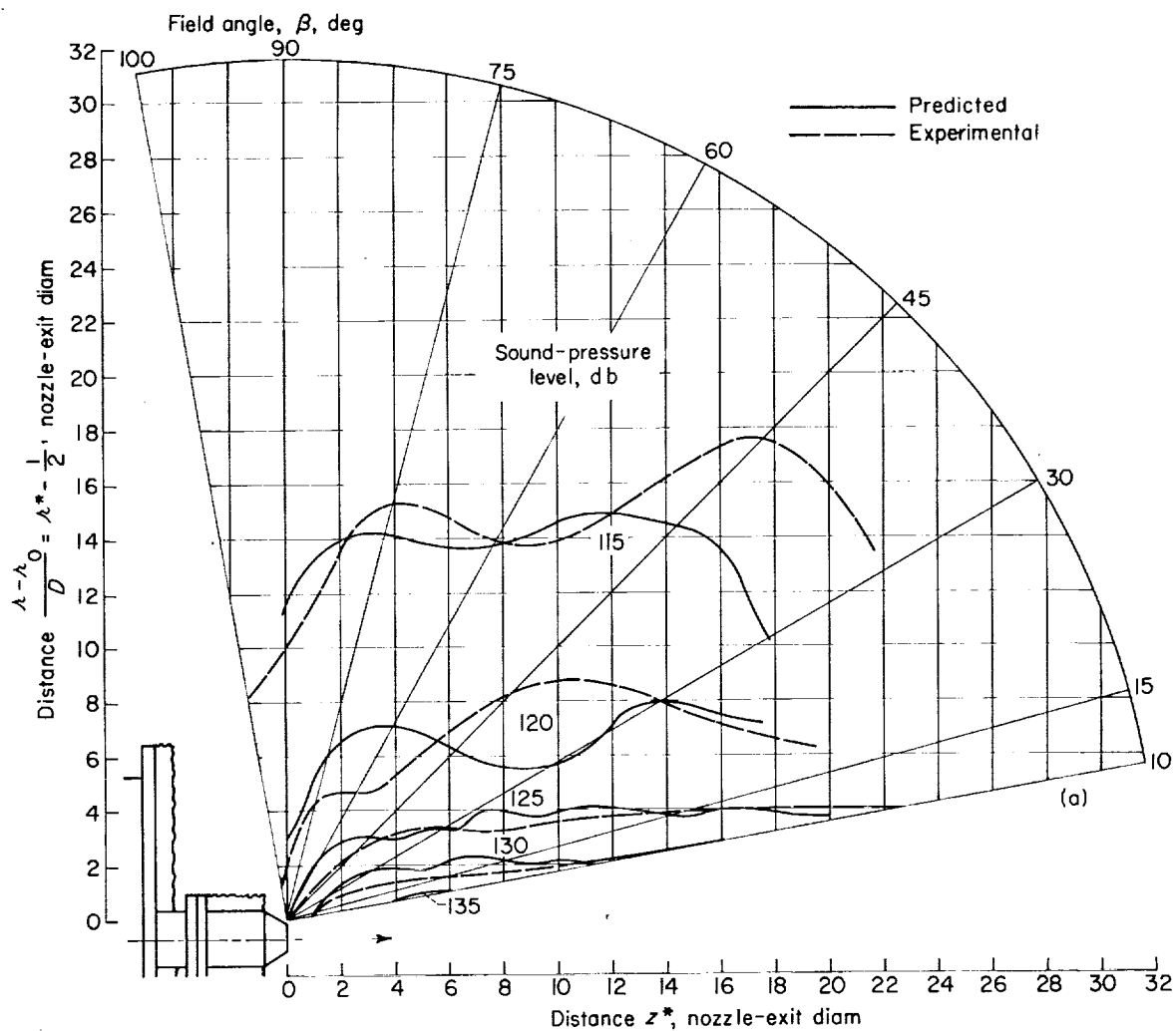
(a) Nozzle diameter D, 3 inches; velocity U, 931 feet per second.   Reference D, 3 inches; U, 803 feet per second (fig. 7(a)).

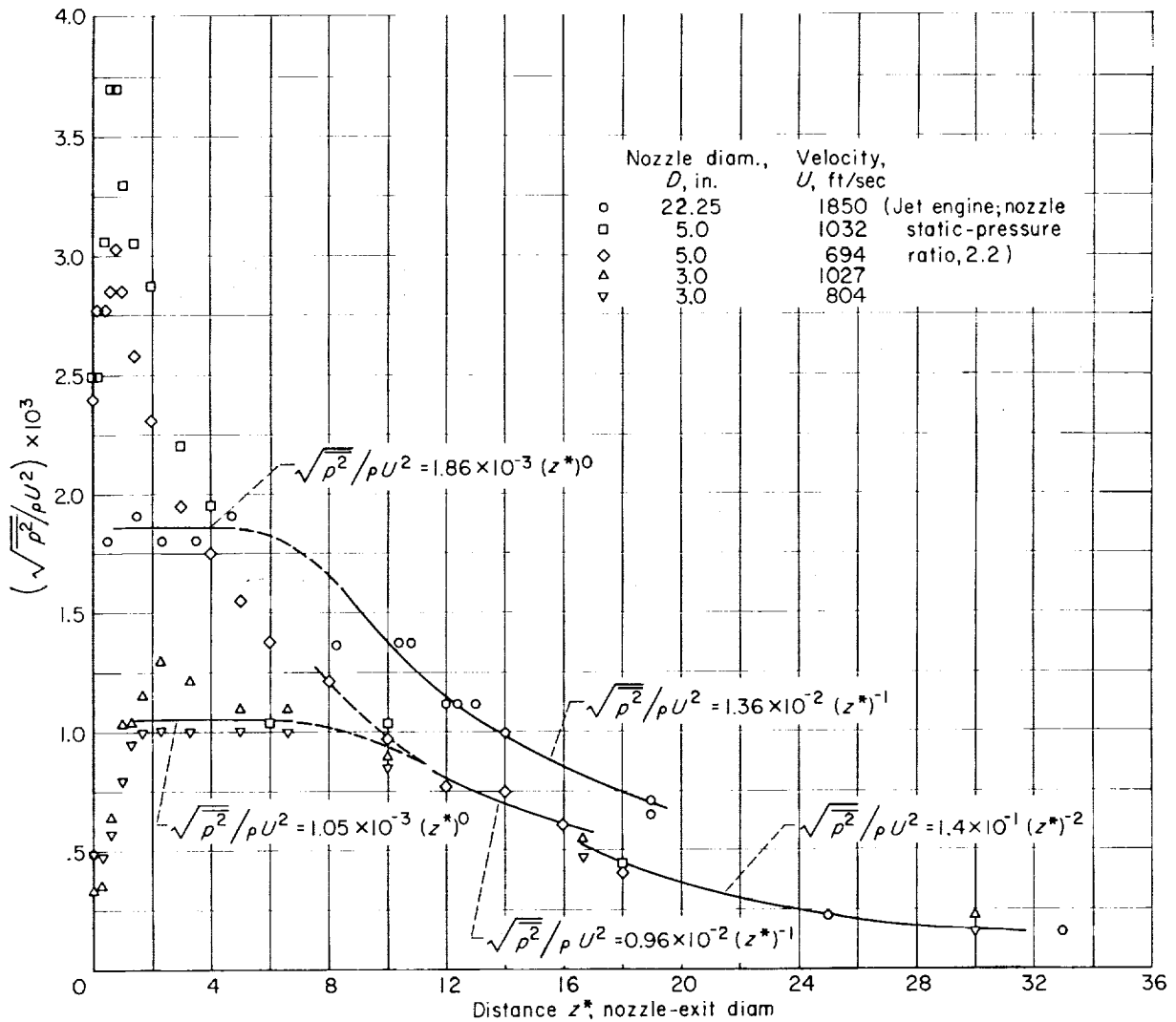FIGURE 11.—Comparison of predicted and experimental overall-sound-pressure-level contours.
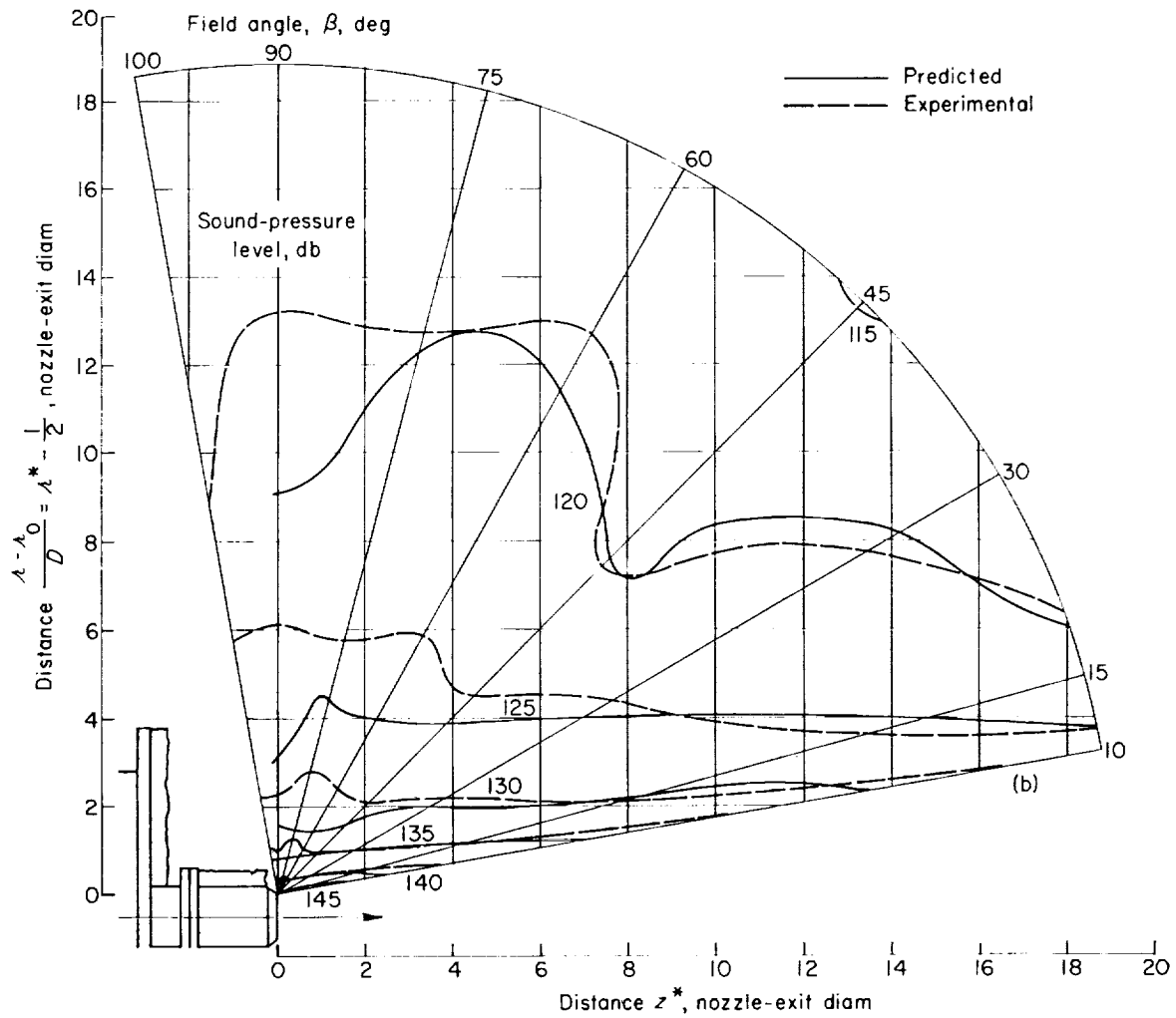
(b) Nozzle diameter D, 5 inches; velocity U, 894 feet per second.   Reference D, 5 inches; U, 690 feet per second
(fig. 8(a)).

FIGURE 11.—Concluded.   Comparison of predicted and experimental overall-sound-pressure-level contours.

FIGURE 12.—Dimensionless fluctuation-pressure profiles along mean-velocity boundary of jet.

relatively large azimuth. A representation of contours in terms of pressure fluctuations in passbands (cf. eqs. (11) and (12)) would also have been permissible because the values of Strouhal number corresponding to the filter cutoff frequencies were nearly equal.

The spacewise distribution of n for overall pressure fluctuations was depicted in figure 9. Because the effective geometry of a jet as a noise source is a function of frequency, it appears quite likely that the distribution of n is also a function of frequency. The data shown in the reference maps (figs. 13 and 14) were used to determine the distributions of the jet velocity exponent ν, the spectral-density correspondent of n (cf. eqs. 3(a) and 7(a)), for a relatively large and for

a relatively small value of Strouhal number. Distributions for the 5- and 3-inch-diameter nozzles are shown in figures 16 and 17, respectively. (Because the microphone-response correction for $f=20$ kc was not known, the distribution of the exponent ν for $D=3$ in., $\nu_m \approx 5$ could not be reliably determined.) Over small regions, values of the exponent ν of less than 2 and greater than 8 were obtained. Values of the exponent ν tended to be smallest along the jet boundary, especially near the nozzle. However, because the measurements of filtered signals were less accurate than measurements of unfiltered signals (simply because of the reduced bandwidth), a number of repetitions of the tests would be necessary before definite conclusions could be reached.
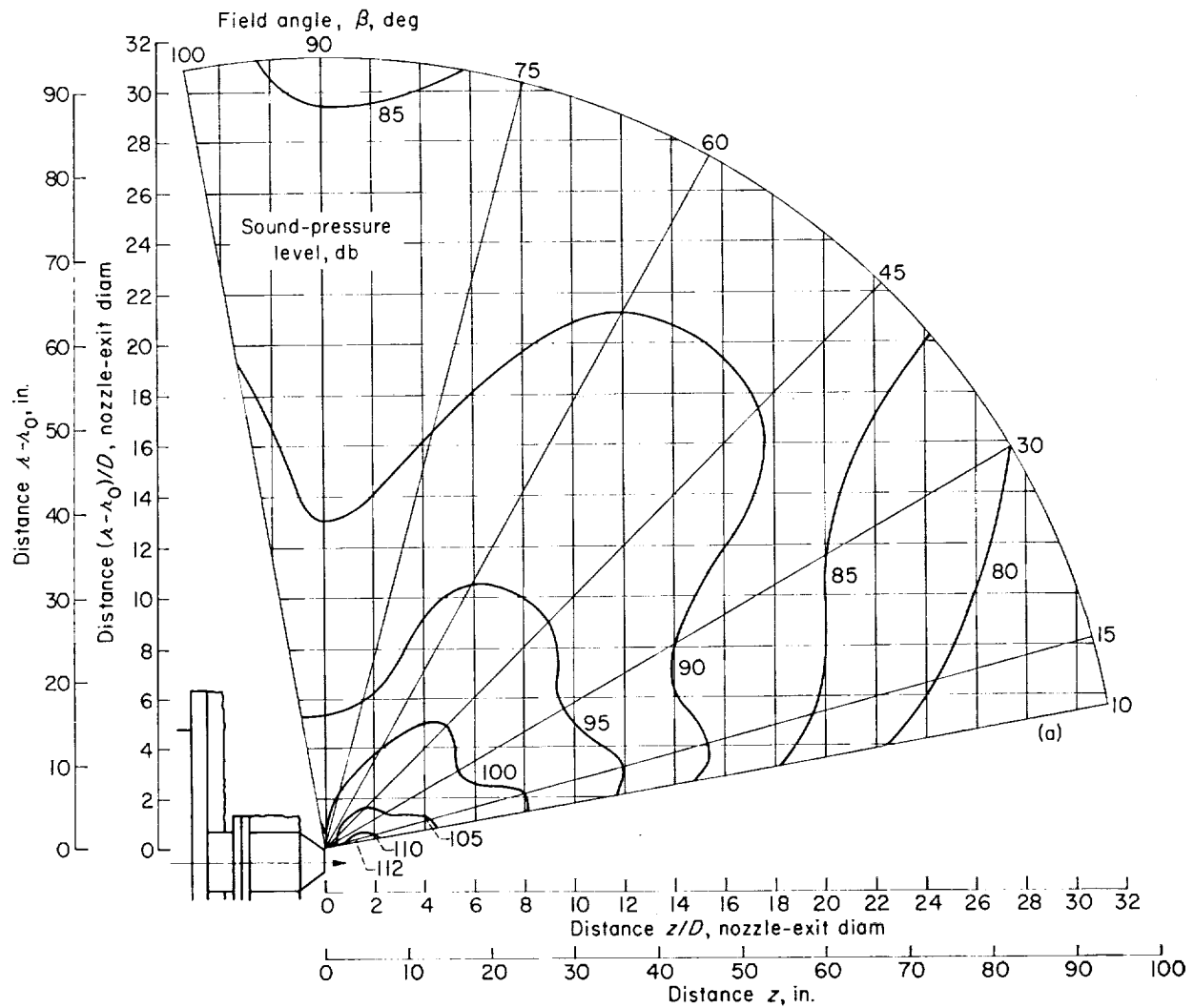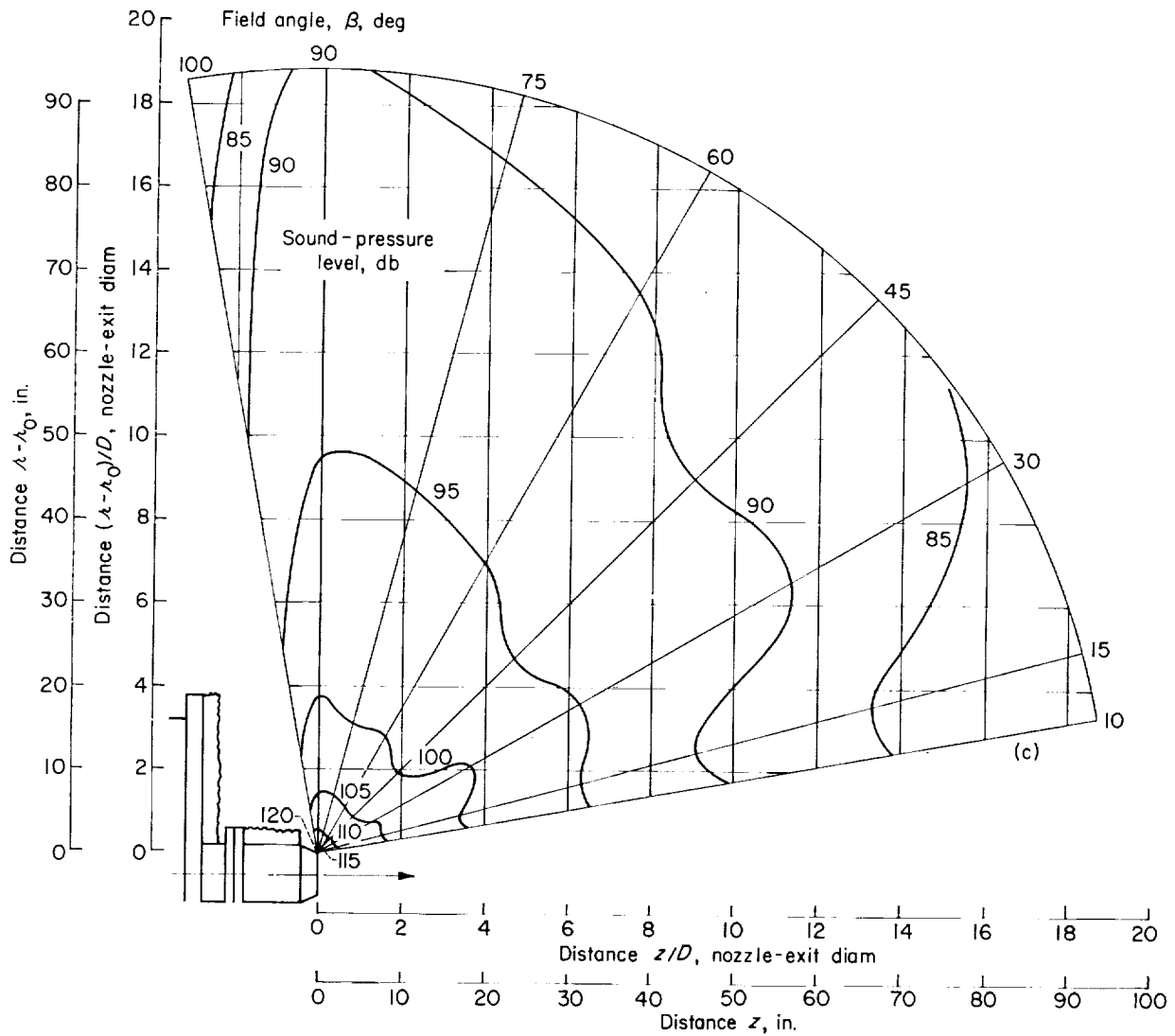
(a) Nozzle diameter D, 3 inches; velocity U, 803 feet per second; $f_m = 16,000$ cycles per second; $\nu_m = 4.99$.

FIGURE 13.—Contours of sound-pressure level in one-third-octave bands for subsonic jets. Strouhal number large
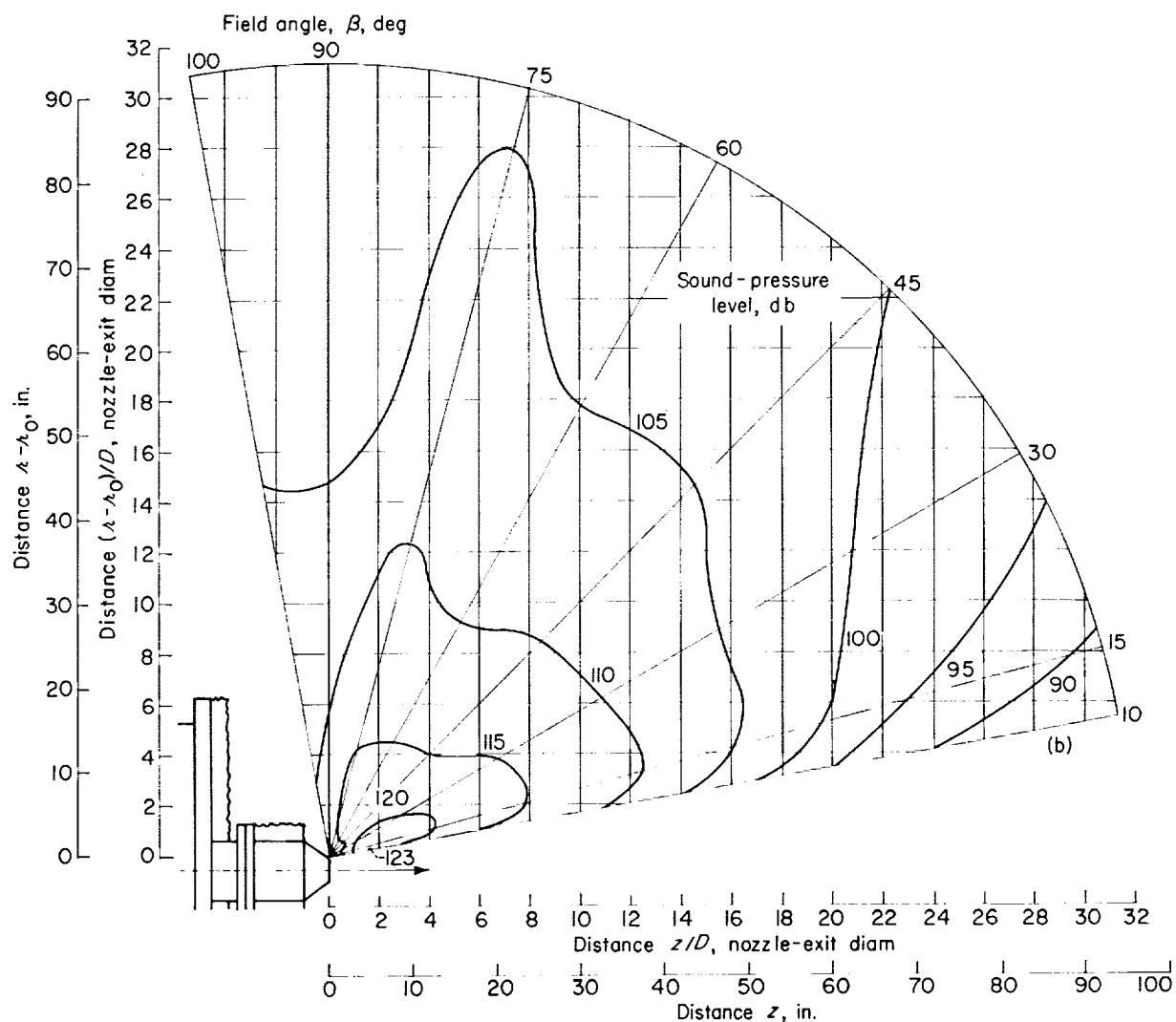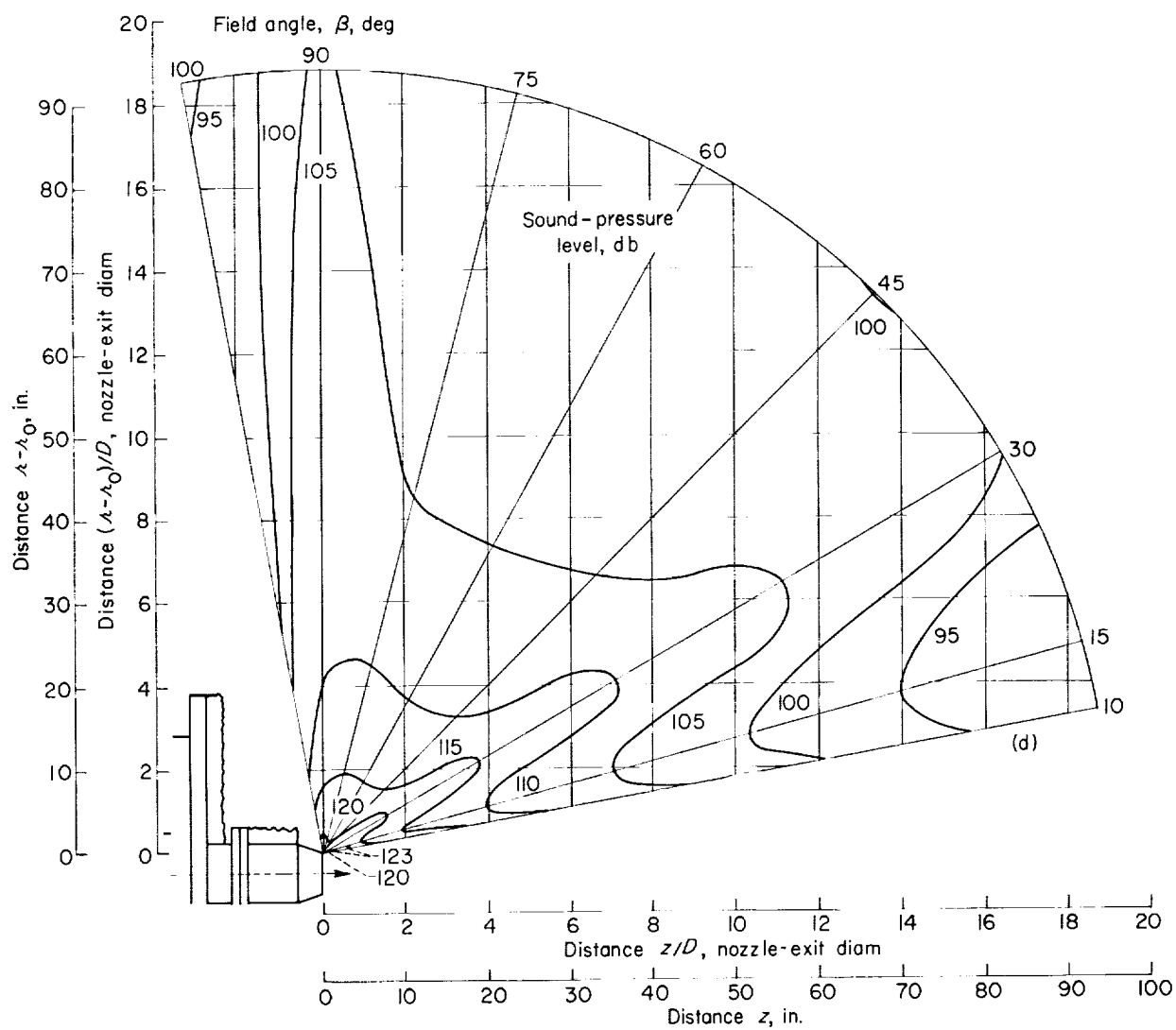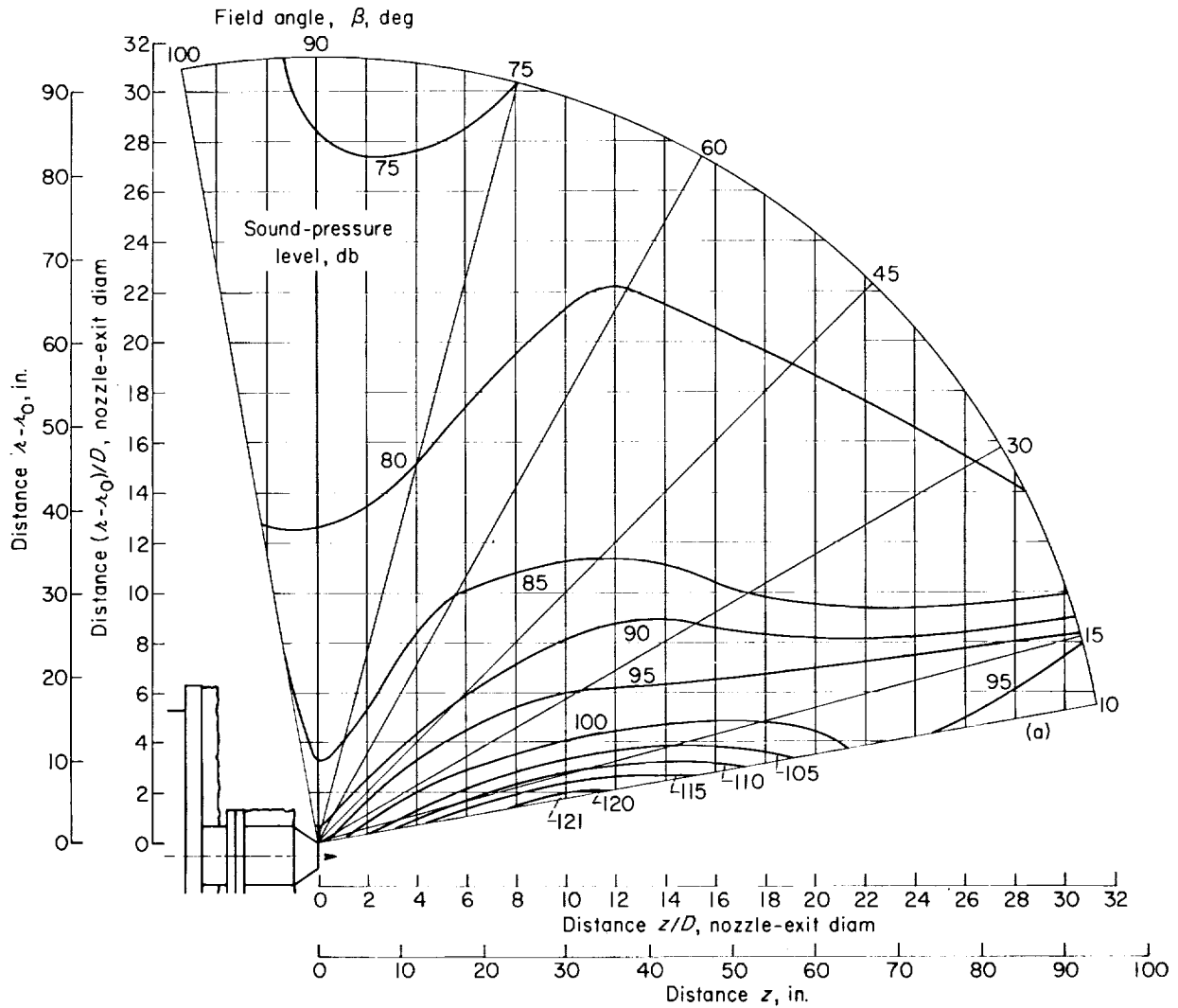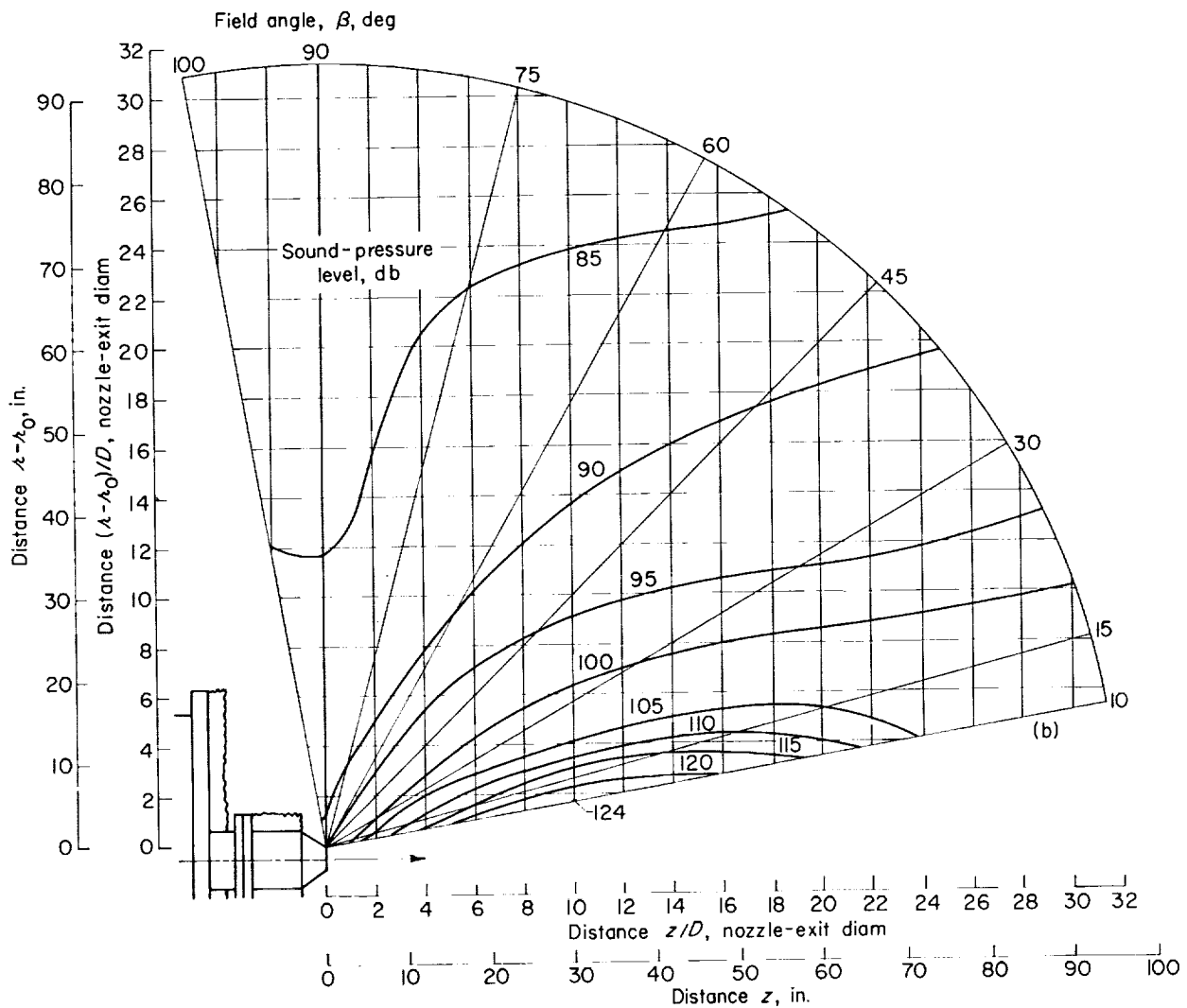
(b) Nozzle diameter D, 3 inches; velocity U, 1021 feet per second; $f_m = 20{,}000$ cycles per second; $\nu_m = 4.88$.   (No frequency response correction.)

FIGURE 13.—Continued.   Contours of sound-pressure level in one-third-octave bands for subsonic jets.   Strouhal number large.

(c) Nozzle diameter D, 5 inches; velocity U, 690 feet per second; $f_m = 8000$ cycles per second; $\nu_m = 4.83$.

FIGURE 13. Continued. Contours of sound-pressure level in one-third-octave bands for subsonic jets. Strouhal number large.
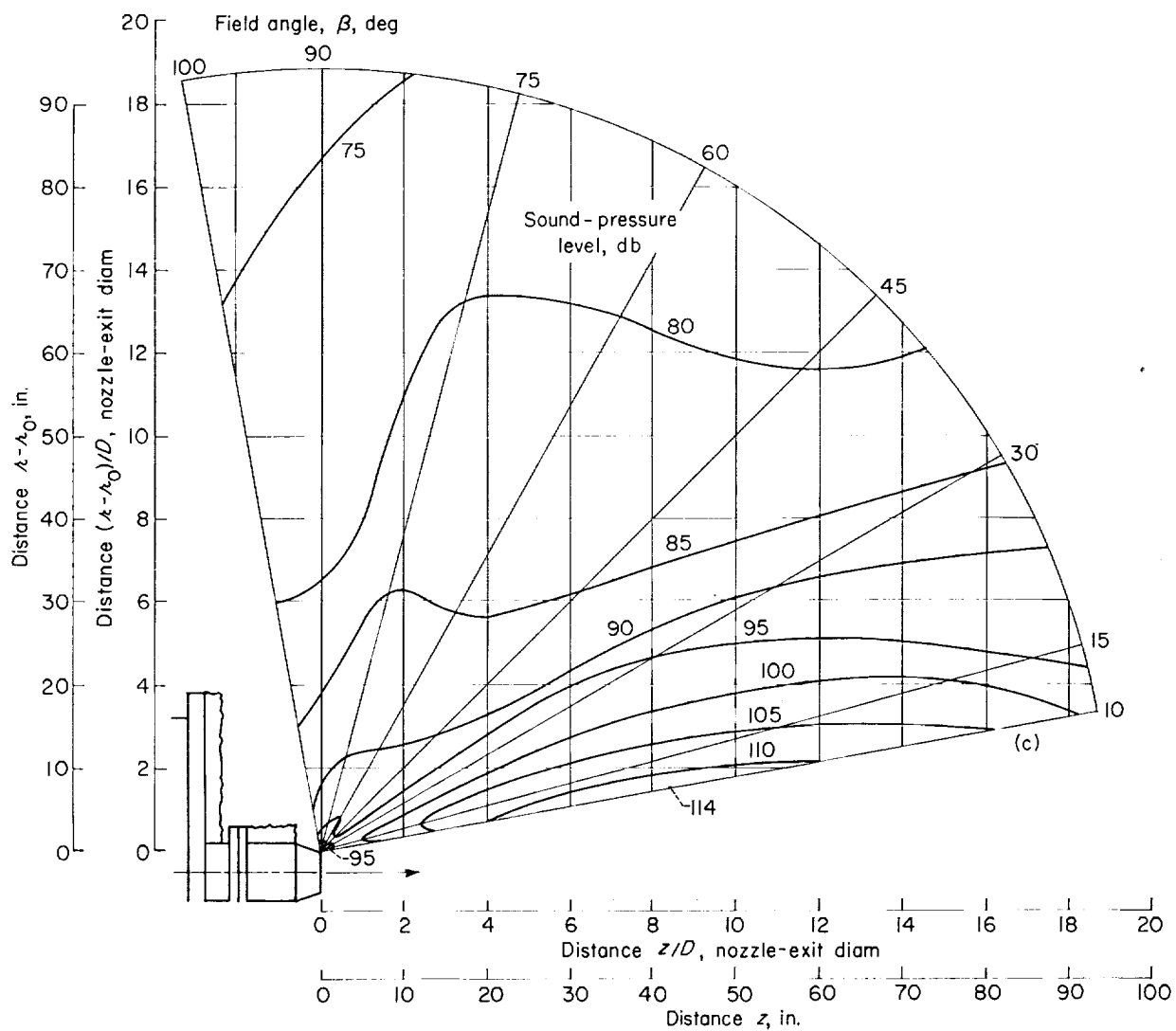
(d) Nozzle diameter D, 5 inches; velocity U, 1028 feet per second; $f_m = 12{,}500$ cycles per second; $\nu_m = 5.06$.

FIGURE 13.—Concluded. Contours of sound-pressure level in one-third-octave bands for subsonic jets. Strouhal number large.

(a) Nozzle diameter D, 3 inches; velocity U, 803 feet per second; $f_m = 200$ cycles per second; $\nu_m = 0.0624$.

FIGURE 14.—Contours of sound-pressure level in one-third-octave bands for subsonic jets. Strouhal number small.
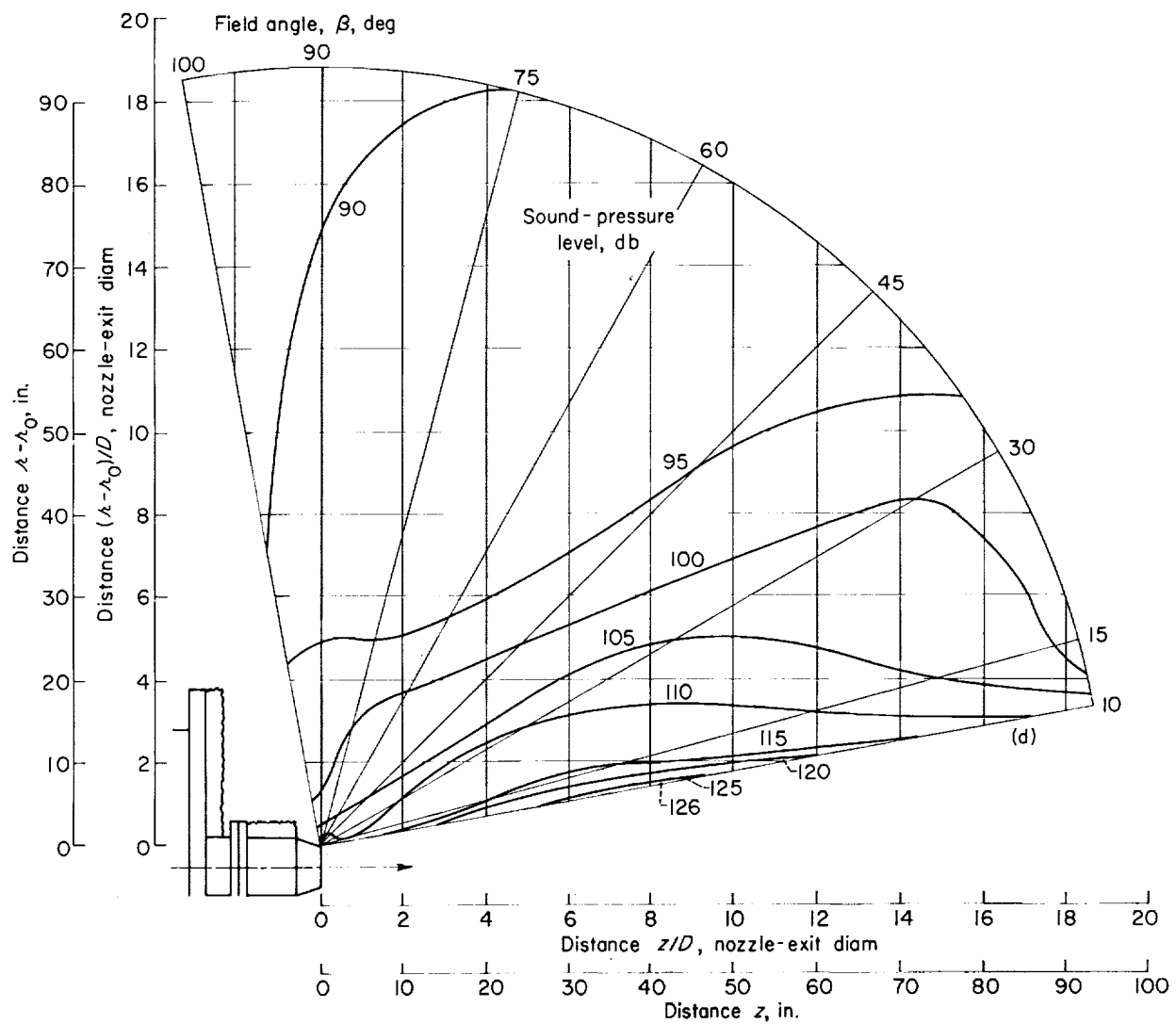
(b) Nozzle diameter D, 3 inches; velocity U, 1021 feet per second; $f_m = 250$ cycles per second; $\nu_m = 0.0610$.

FIGURE 14.—Continued.   Contours of sound-pressure level in one-third-octave bands for subsonic jets.   Strouhal number small.
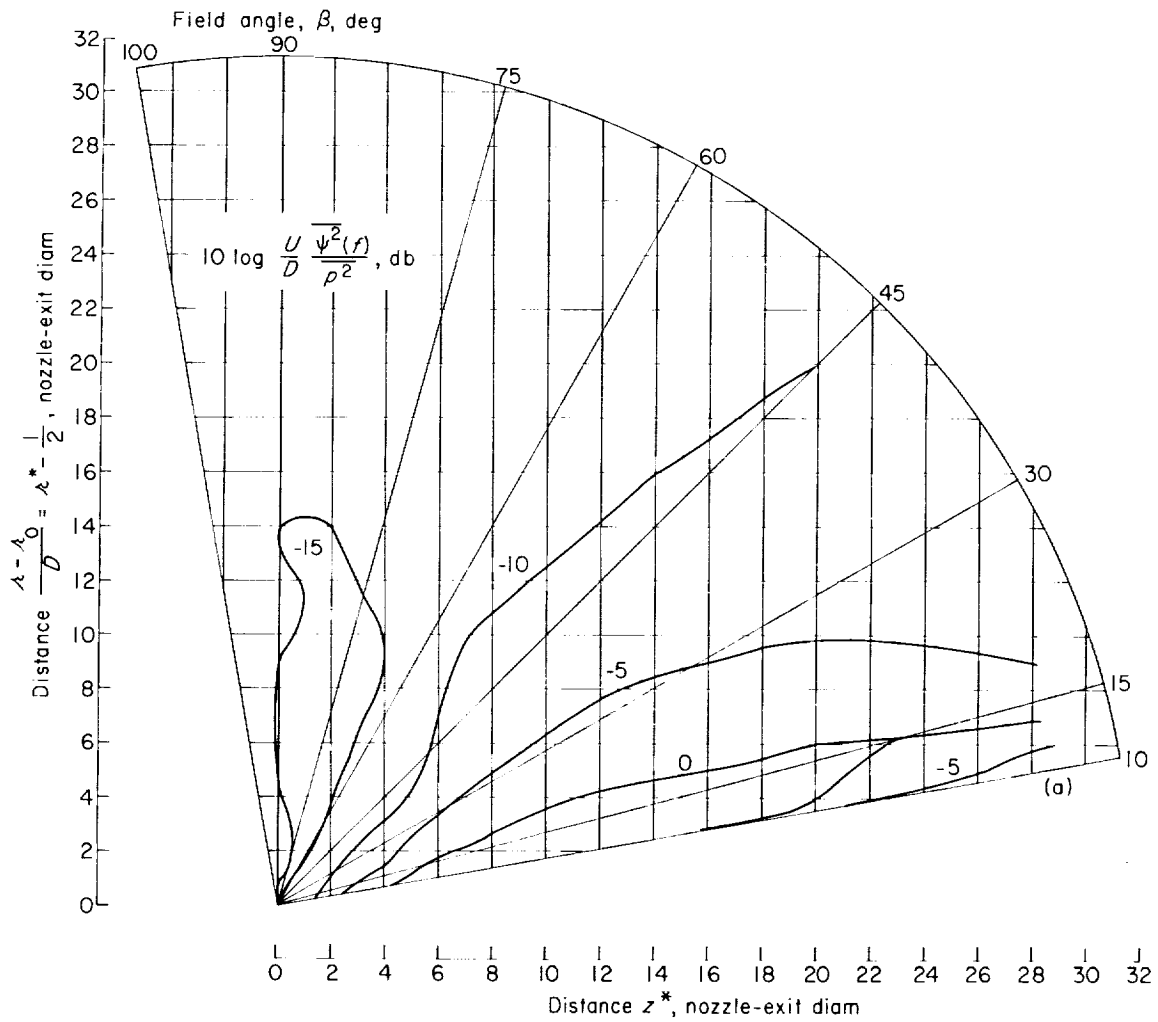
(c) Nozzle diameter D, 5 inches; velocity U, 690 feet per second; $f_m = 100$ cycles per second; $\nu_m = 0.0604$.

FIGURE 14.—Continued. Contours of sound-pressure level in one-third-octave bands for subsonic jets. Strouhal number small.
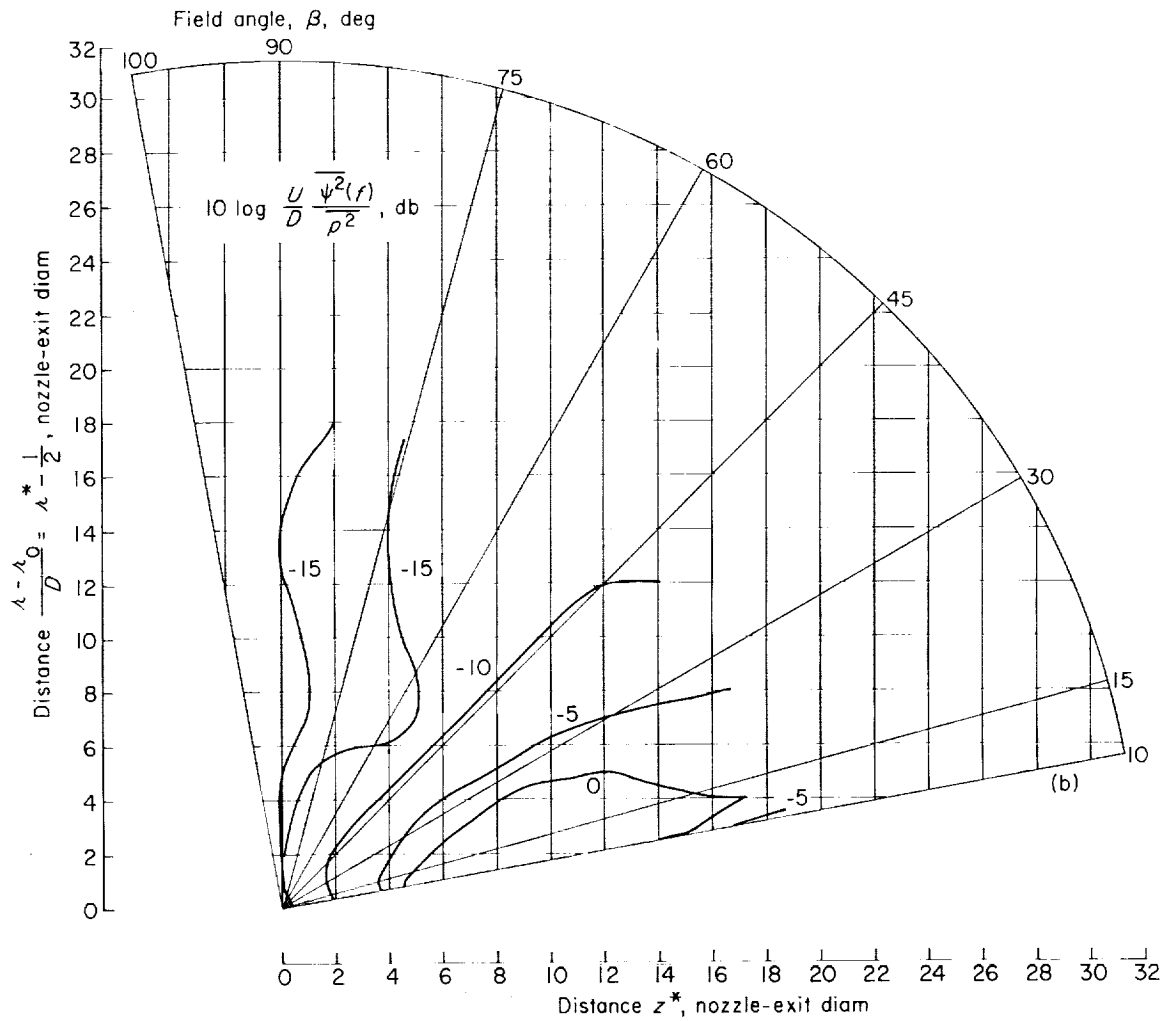
(d) Nozzle diameter D, 5 inches; velocity U, 1028 feet per second; $f_m = 160$ cycles per second; $\nu_m = 0.0648$.

FIGURE 14.—Concluded. Contours of sound-pressure level in one-third-octave bands for subsonic jets. Strouhal number small.
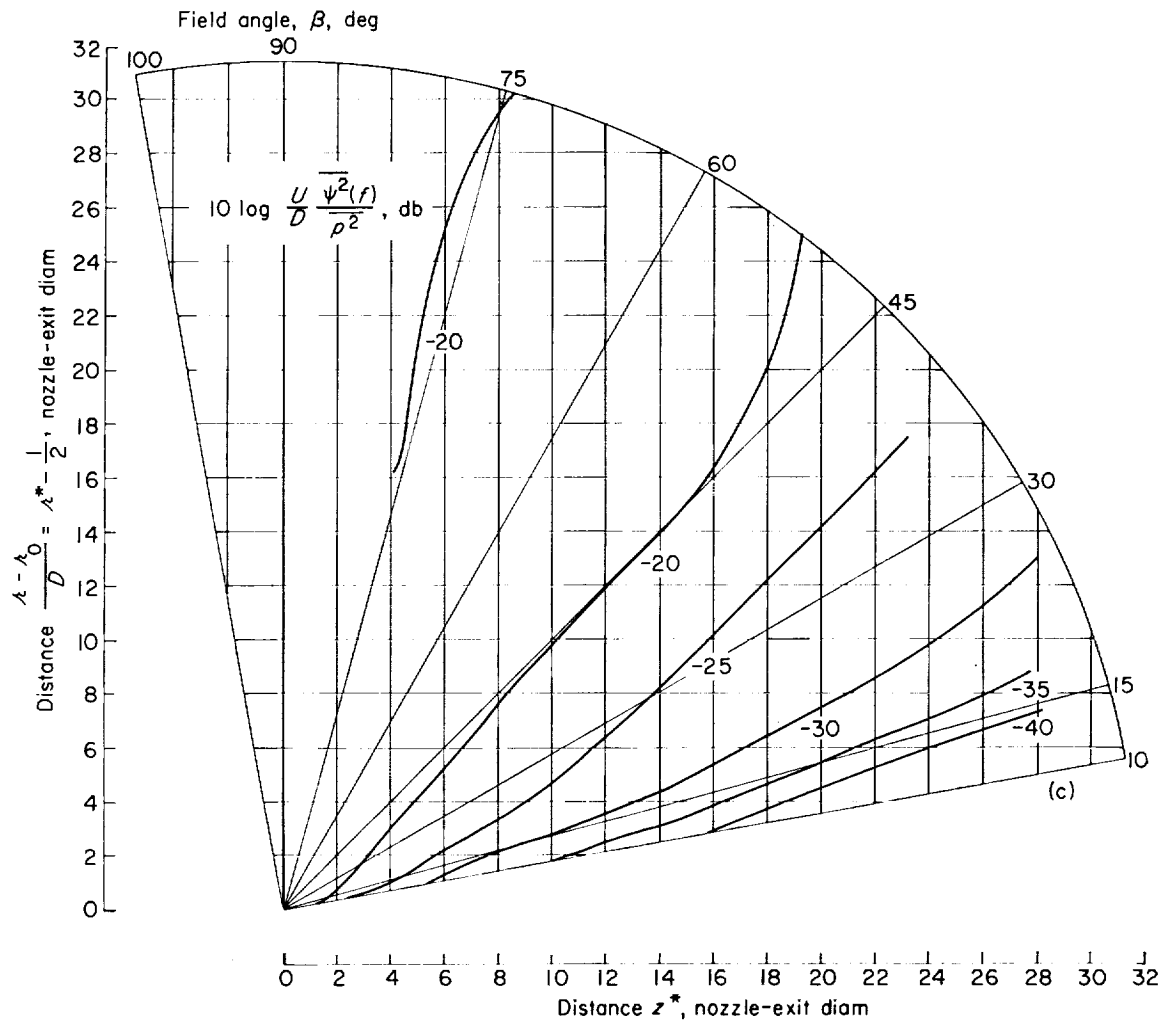
(a) $\nu_m \approx 0.062$; nozzle diameter D, 3 inches. (Velocity U, 803 and 1021 ft/sec.)

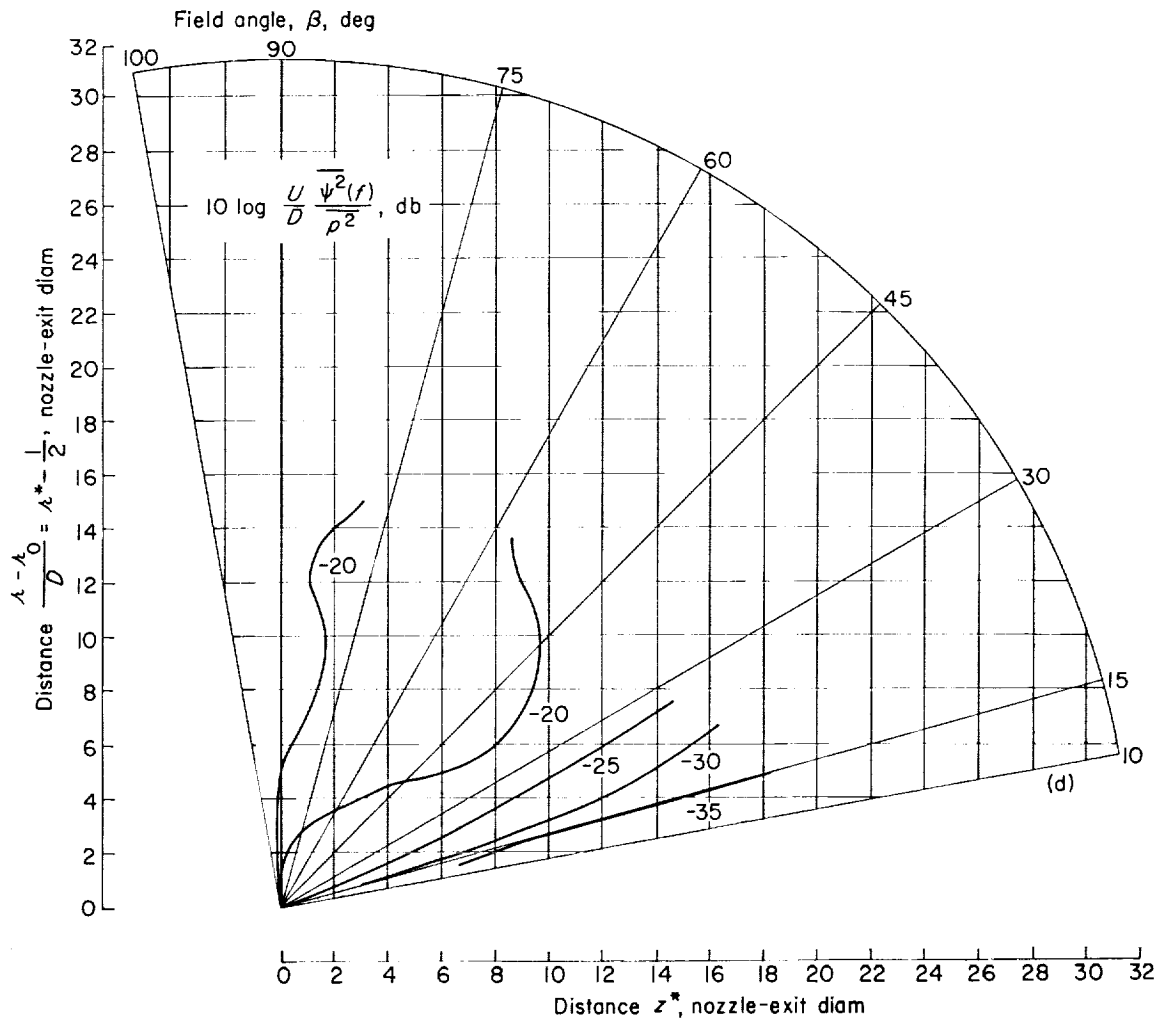FIGURE 15.—Contours of dimensionless mean-square-pressure-spectral-density level for subsonic jets.

(b) $\nu_m \approx 0.062$; nozzle diameter D, 5 inches. (Velocity U, 690 and 1028 ft/sec.)

FIGURE 15.—Continued. Contours of dimensionless mean-square-pressure-spectral-density level for subsonic jets.
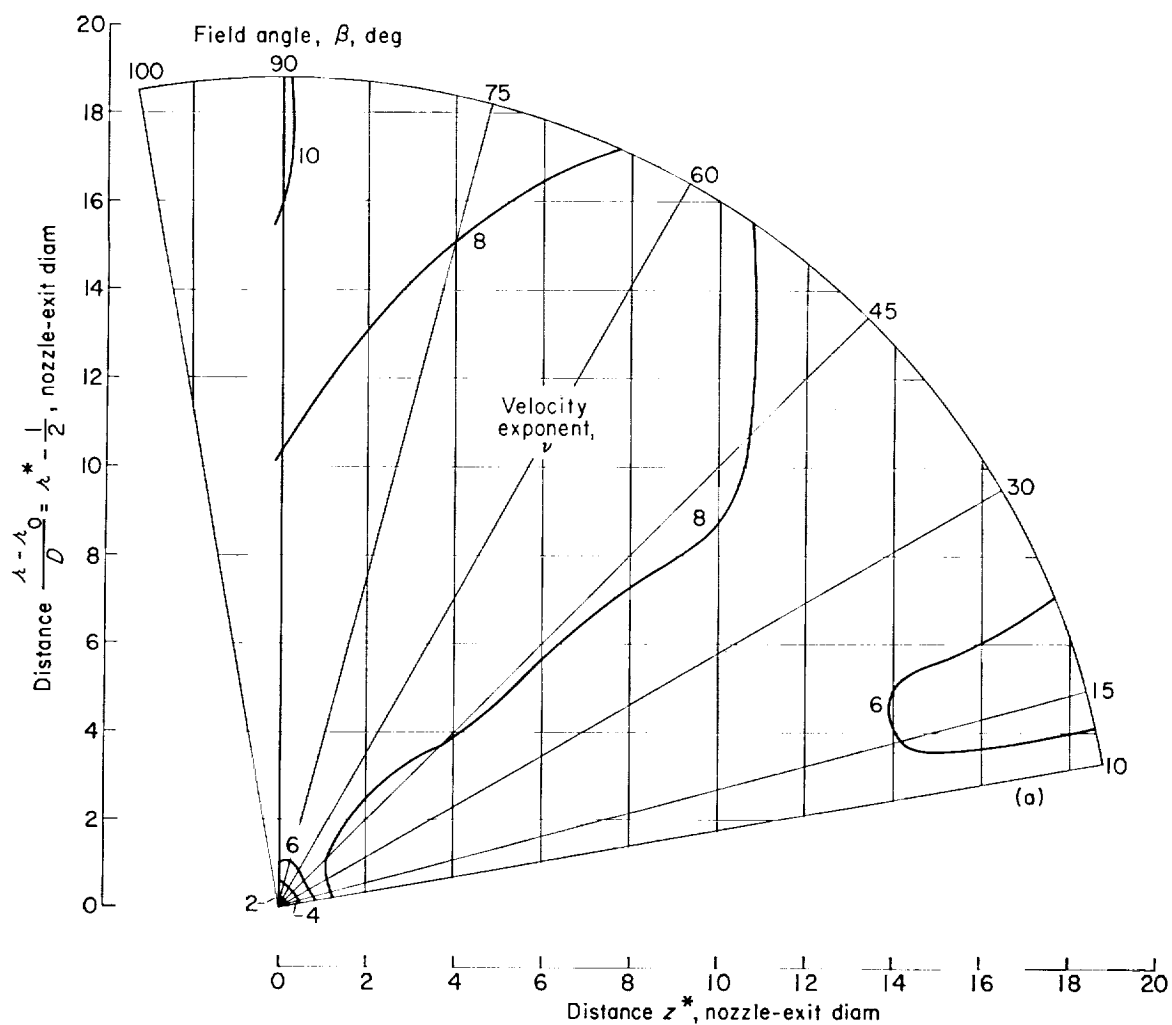
(c) $\nu_m \approx 4.9$; nozzle diameter D, 3 inches. (Velocity U, 803 and 1021 ft/sec.)

FIGURE 15.—Continued. Contours of dimensionless mean-square-pressure-spectral-density level for subsonic jets.
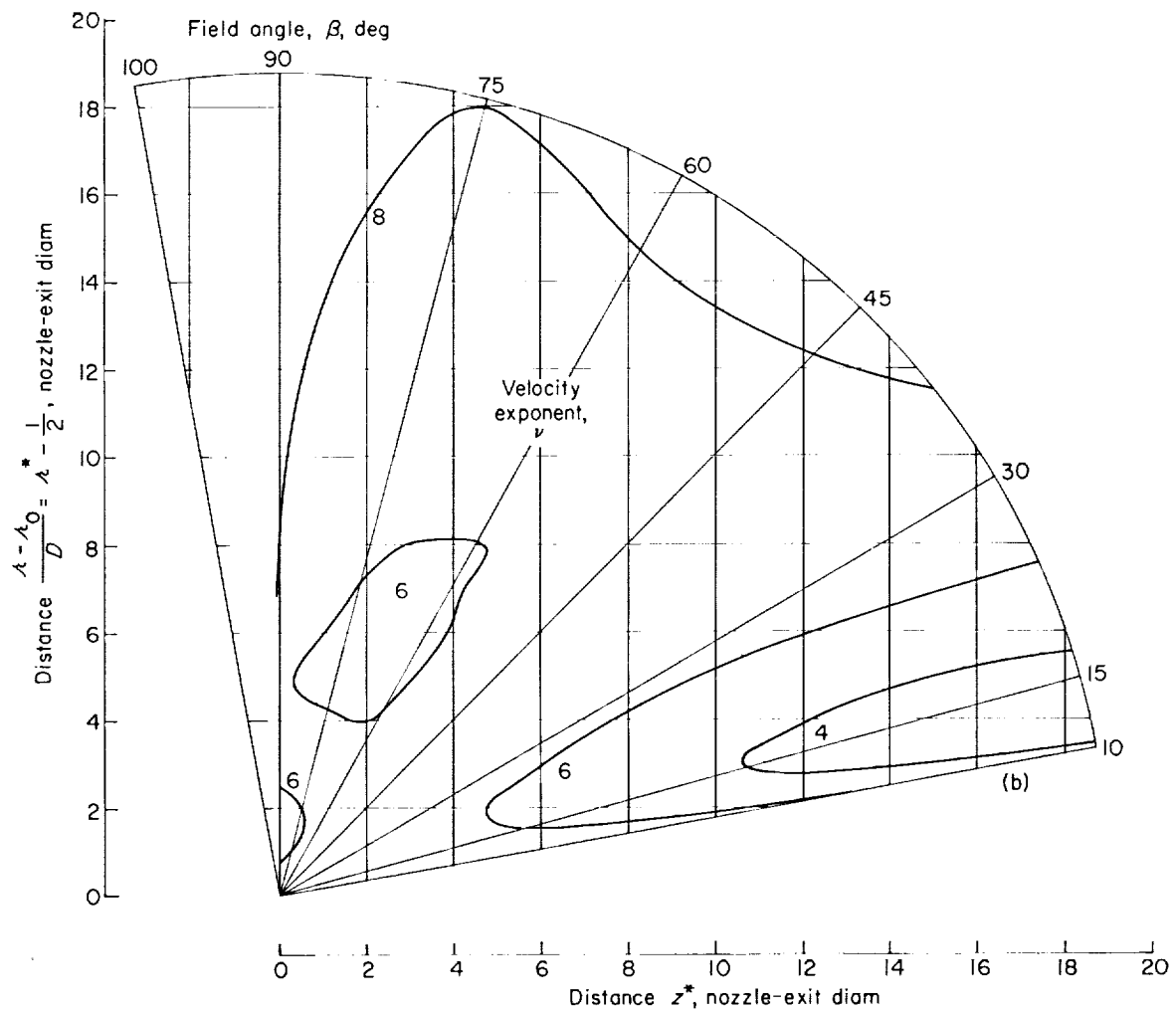
(d) $\nu_m \approx 4.9$; nozzle diameter D, 5 inches.   (Velocity U, 690 and 1028 ft/sec.)

FIGURE 15.—Concluded.   Contours of dimensionless mean-square-pressure-spectral-density level for subsonic jets.

(a) Nozzle diameter D, 5 inches; $\nu_m \approx 5$.

FIGURE 16.—Distribution of exponent ν for frequency pass-bands.

(b) Nozzle diameter D, 5 inches; $\nu_m \approx 0.06$.

FIGURE 16.—Concluded.   Distribution of exponent ν for frequency pass-bands.
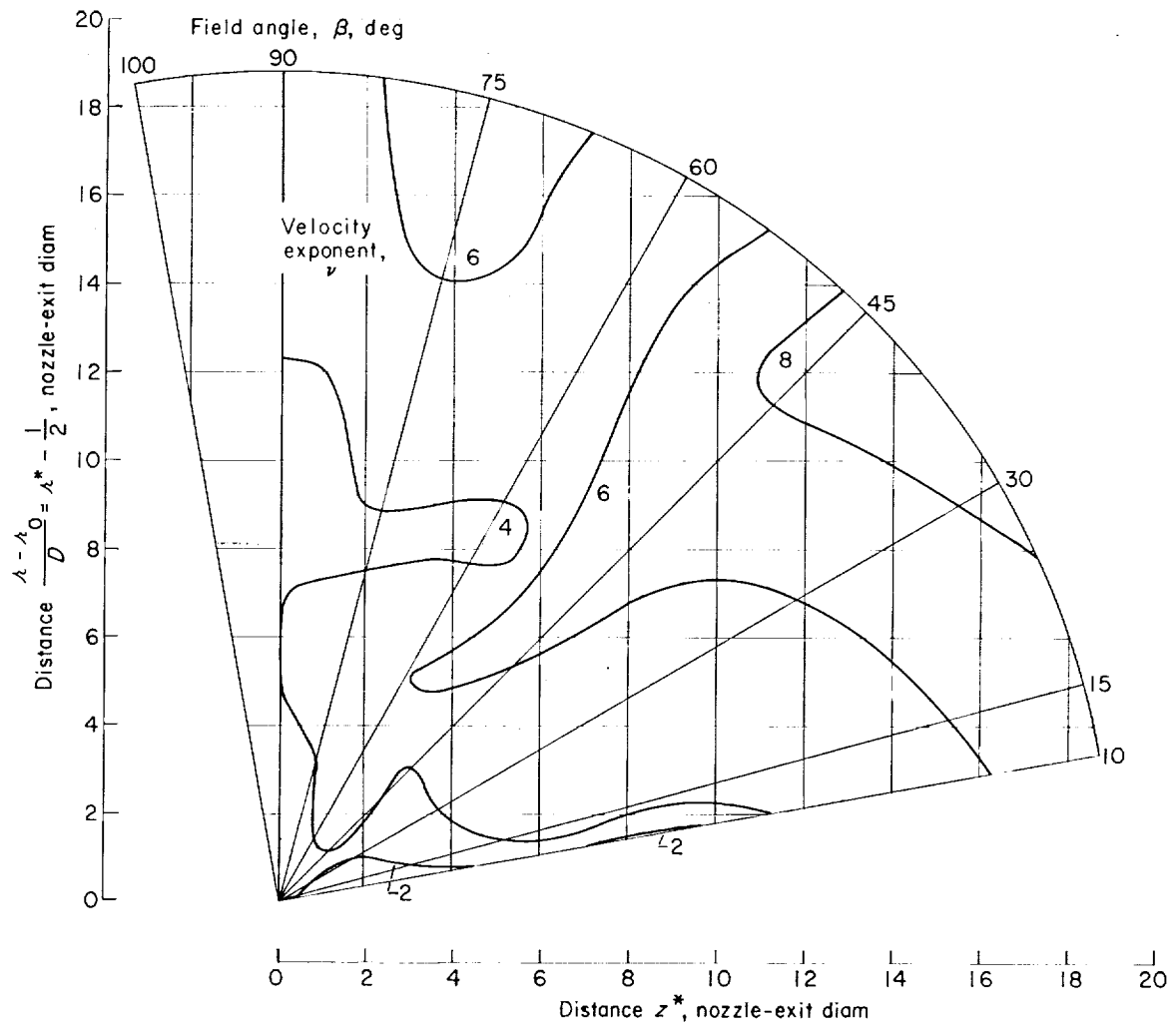
FIGURE 17.—Distribution of exponent ν for frequency pass-bands. Nozzle diameter D, 3 inches; $\nu_m \approx 0.06$.

The reference maps (figs. 13 and 14) in conjunction with the computed distributions of the exponent ν were used to predict the sound-pressure-level field for the 5-inch-diameter nozzle at an intermediate value of velocity ($U=894$ ft/sec). Predictions were made for both values of Strouhal number. The predicted maps were computed in the same manner as were those for overall-sound-pressure level. The predicted contours, shown in figure 18, are in relatively good agreement with the experimentally determined contours, also shown in figure 18.

In figure 19 the distribution along the jet boundary of pressure fluctuations in frequency pass-bands is shown in dimensionless form for the 3- and 5-inch-diameter nozzles. Although the nozzle contours differ, there is a general similarity of the profiles of the pressure fluctuations. The similarity is somewhat poorer for the higher frequencies, which are generated nearer the nozzle and, hence, should be most seriously affected by the nozzle profile. For each nozzle a systematic difference among the profiles is observed. For the smaller values of Strouhal number ($\nu_m \lesssim 0.1$), the spectral-density level for the lesser value of jet velocity is generally slightly higher than that for the greater value of velocity. For the larger values of Strouhal number ($\nu_m \gtrsim 1$), the situation is reversed, that is, the spectral-density level for the greater value of jet velocity is significantly higher. It seems possible that a slight dissimilarity of the jet exit-velocity profile over the subsonic range might account for the observed effect.

The loci of maxima of the fluctuation-pressure profiles for each frequency band are plotted in dimensionless form in figure 20. The maxima referred to are, however, spectral-density, or spectrum-level, maxima, not the dimensionless spectral-density maxima which would be obtained from figure 19. The loci of the two sets of maxima differ because $\overline{p^2}$ is a function of the dimensionless axial coordinate z^*. The loci shown in figure 20 are of greater interest because of their possible application in connection with the theory presented in reference 10.

Although the loci in figure 20 agree generally with those previously established for round jets

(refs. 13 and 10), in certain intervals of z^* the various determinations differ by a measurable amount. In this regard some important differences exist among the various tests. For example, figure 20 applies to cold subsonic jets and the nozzles sketched in figure 4. The fluctuation-pressure results in reference 13 (fig. 17) apply to a turbojet engine operated at a supercritical value of nozzle pressure ratio. The results of Dyer and Franken (ref. 10) apply to a large rocket. Considering the wide divergency of test conditions, the good agreement of the loci is surprising.

There were other important experimental differences involved in determining the loci of the "noise sources." The loci shown in figure 20 and reference 13 (fig. 17) were established from measurements of near-field noise, hence pressure fluctuations associated with incompressibility (pseudosound), whereas those in reference 10 were determined from measurements of far-field pressure fluctuations associated with compressibility (sound). Specifically, determinations of noise source location from far-field tests should apply in Dyer's theory (ref. 10). However, because the acoustic radiation is driven by the essentially incompressible, near-field, pressure fluctuations (ref. 18), it might be presumed (cf. ref. 19, eq. II 7) that relatively high pseudosound levels are associated with relatively high sound levels at the same point. (Sound results if the second time derivatives of the pseudosound pressures in a coordinate system translated at the mean convective velocity of the fluctuations are time-dependent. If sound is radiated, increased amplitudes of the pseudosound-pressure fluctuations lead to increased amplitude of the sound.) Thus, measurements of the incompressible fluctuations might be equally suitable for determining noise source locations. This is borne out by the fact that loci determined by measuring pseudosound- and sound-pressure fluctuations tend to agree. Some disagreement between the two methods of determination exists for $z^* > 10$, but this likely results from certain experimental difficulties encountered in the determination reported in reference 10 (personal communication from Dr. Dyer).
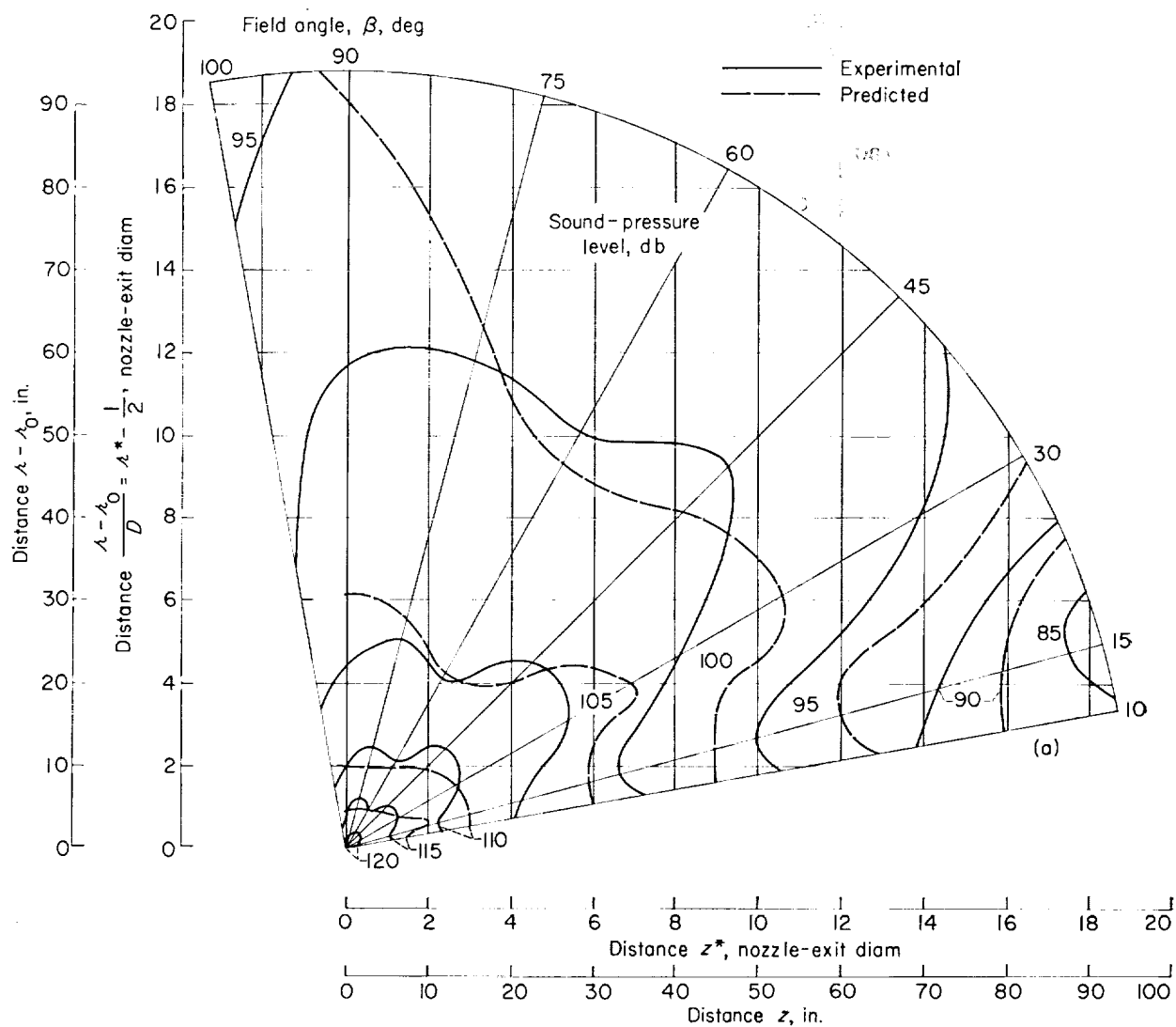
(a) $\nu_m \approx 5$; nozzle diameter D, 5 inches.

FIGURE 18.—Comparison of predicted and experimental contours of sound-pressure level in one-third-octave bands. Velocity U, 894 feet per second.
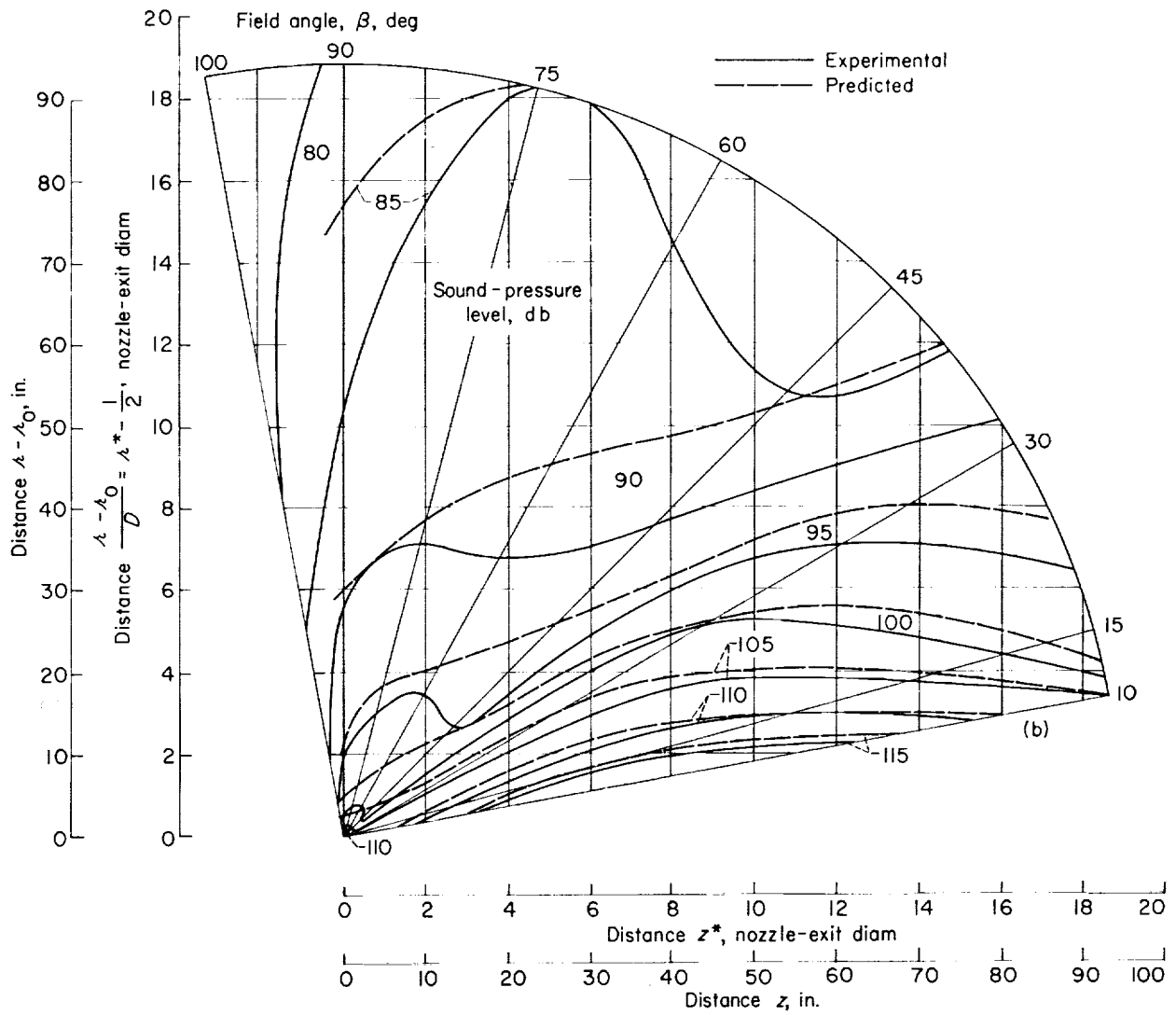
(b) $\nu_m \approx 0.06$; nozzle diameter D, 5 inches.

FIGURE 18.—Concluded. Comparison of predicted and experimental contours of sound-pressure level in one-third-octave bands. Velocity U, 894 feet per second.
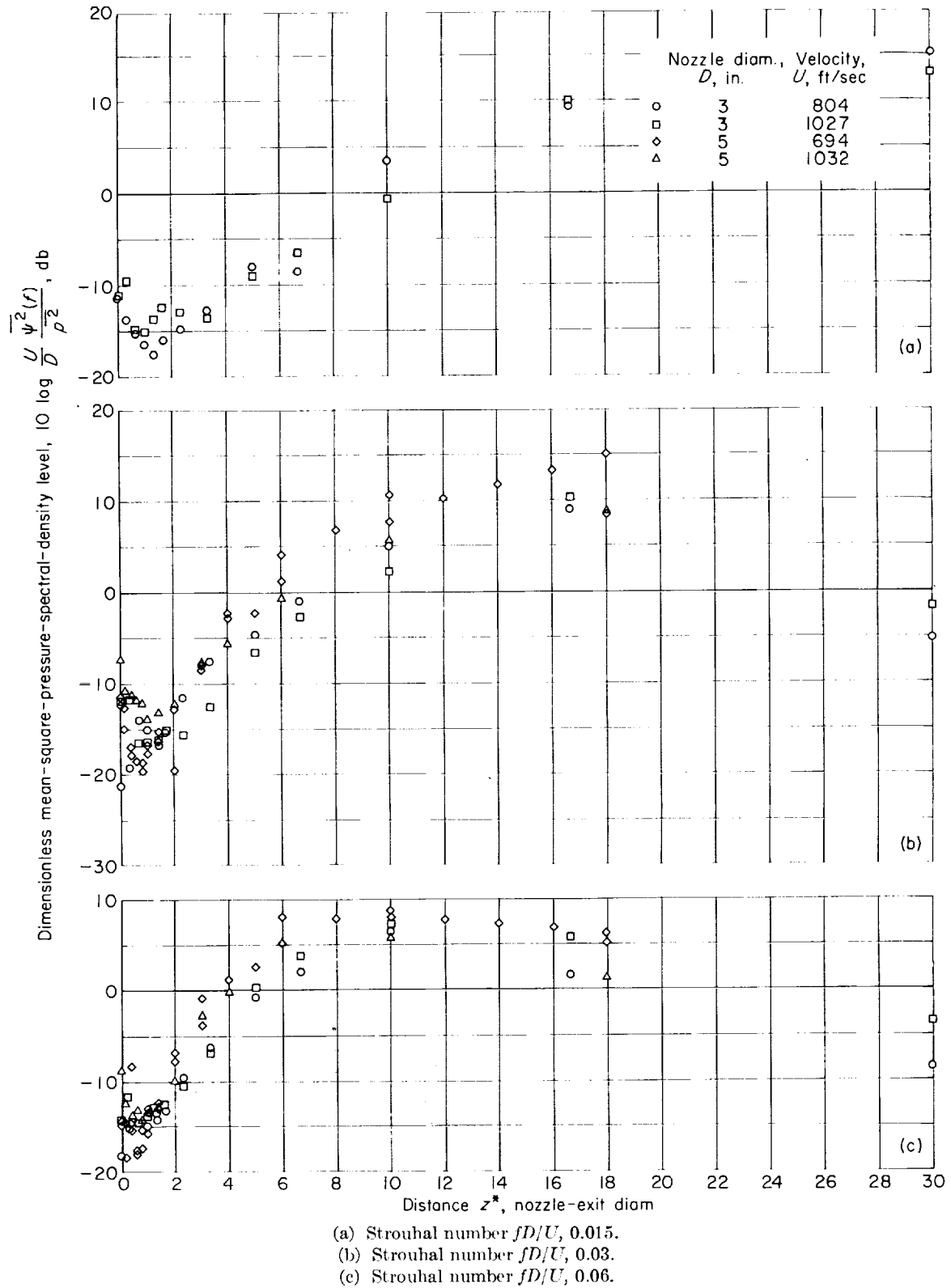
(a) Strouhal number fD/U, 0.015.

(b) Strouhal number fD/U, 0.03.

(c) Strouhal number fD/U, 0.06.

FIGURE 19.—Dimensionless profiles of time-averaged pressure-spectral-density along mean-velocity boundary.

(d) Strouhal number fD/U, 0.12.
(e) Strouhal number fD/U, 0.25.
(f) Strouhal number fD/U, 0.50.

FIGURE 19.—Continued.   Dimensionless profiles of time-averaged pressure-spectral-density along mean-velocity boundary.

(g) Strouhal number fD/U, 0.98.
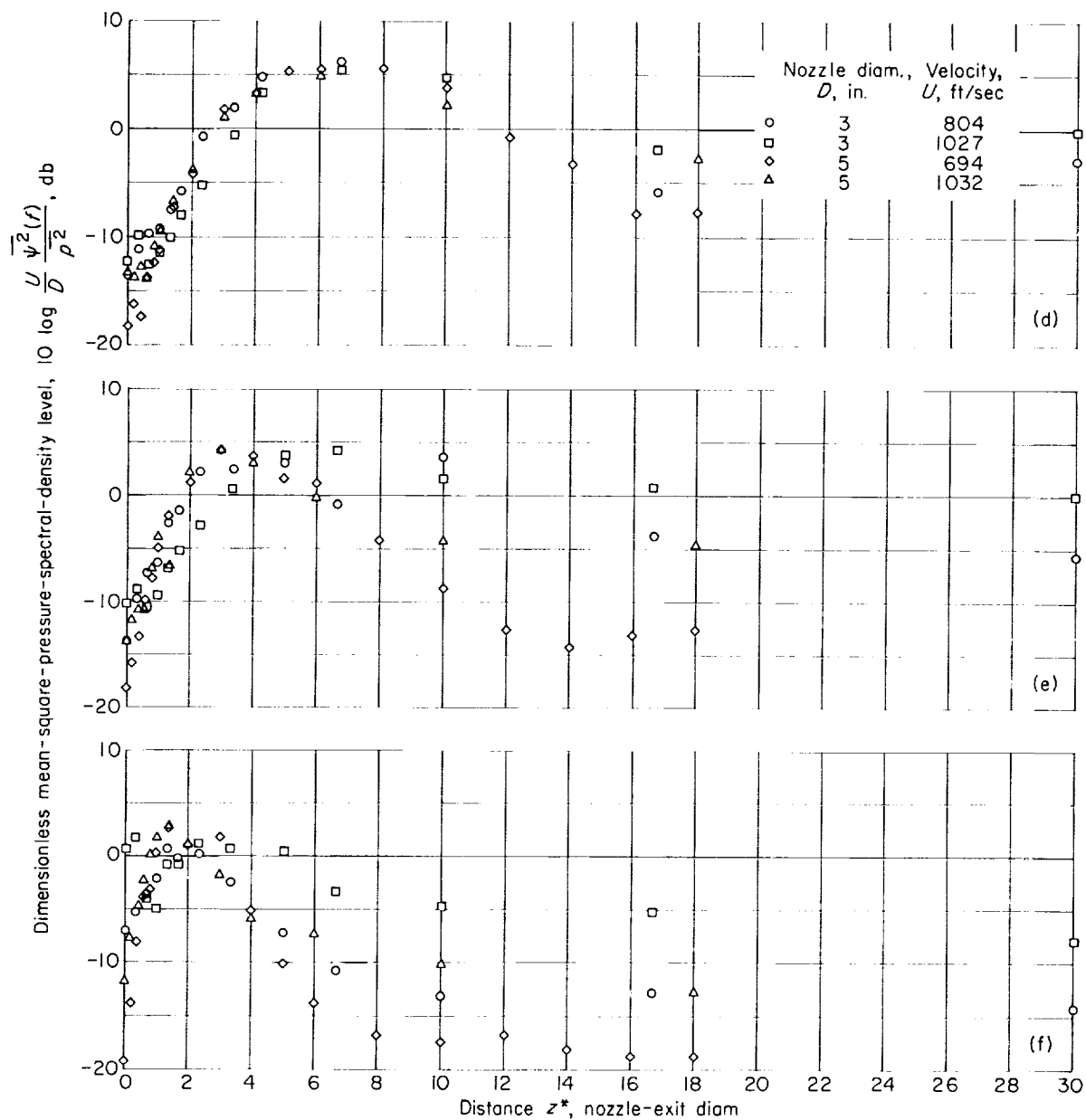(h) Strouhal number fD/U, 1.95.
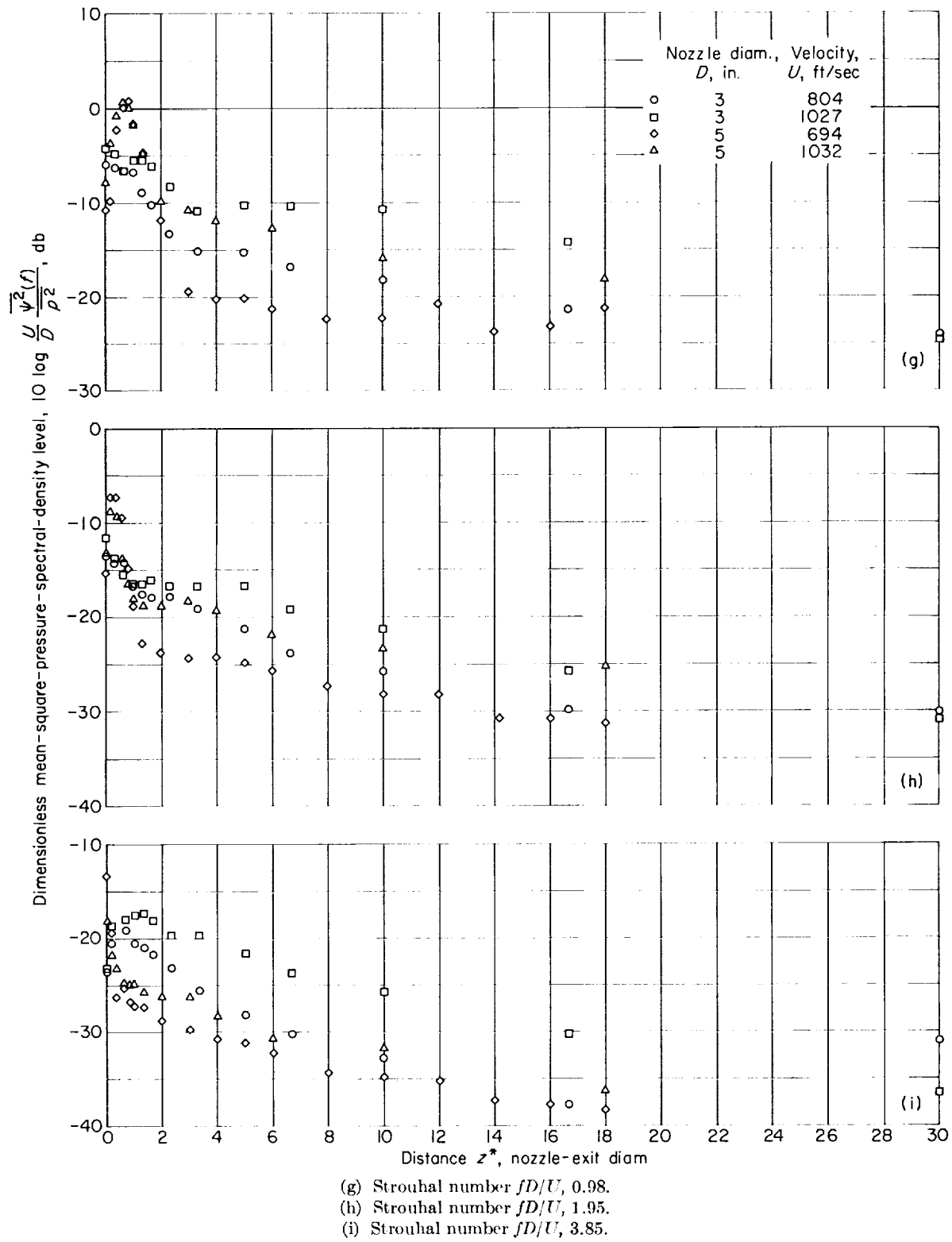(i) Strouhal number fD/U, 3.85.

FIGURE 19.—Concluded.   Dimensionless profiles of time-averaged pressure-spectral-density along mean-velocity boundary.

A difference between the noise source loci associated with the 3- and 5-inch-diameter nozzles is apparent in figure 20. The difference can be qualitatively attributed to the difference between the nozzle profiles. In the case of the 3-inch-diameter nozzle the quasi-laminar boundary layer emerging from the nozzle exit tends to displace the peak fluctuation levels downstream.
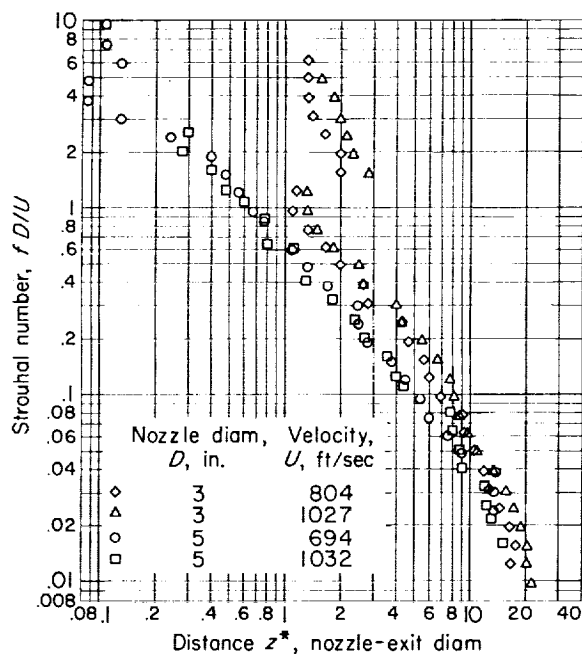

FIGURE 20.—Locus of maxima of fluctuation-pressure profiles for one-third-octave frequency bands.

FLUCTUATION-PRESSURE SPECTRA

Often spectra of pressure fluctuations at discrete points in the noise field are of greater interest than space contours of pressure fluctuations in discrete frequency bands. Several examples of spectra associated with the 3- and 5-inch-diameter nozzles are shown in figure 21. The spectra are presented in the dimensionless form previously discussed.

The spectra for a given nozzle are generally in fair agreement. The greatest disagreement (≈ 5 db) is associated with the 5-inch-diameter nozzle for the larger values of azimuth. The agreement between corresponding results for the two nozzles is generally poor, although agreement tends to improve for smaller values of azimuth and larger values of jet velocity. In general, the trends of the spectra as functions of jet velocity, azimuth, and radial distance have all been noted previously.

Dimensionless spectra along the mean-velocity boundary are shown in figure 22. As expected, the frequency of the spectrum peak decreases as a function of increasing distance downstream of the nozzle exit. The maximum spectral density tends to increase as a function of increasing distance downstream. For all downstream distances, spectra for a given nozzle are in good agreement. However, spectra for the two nozzles do not agree for $z^* < 1$. This is to be expected for nozzles having dissimilar profiles. All spectra possess negative skewness.
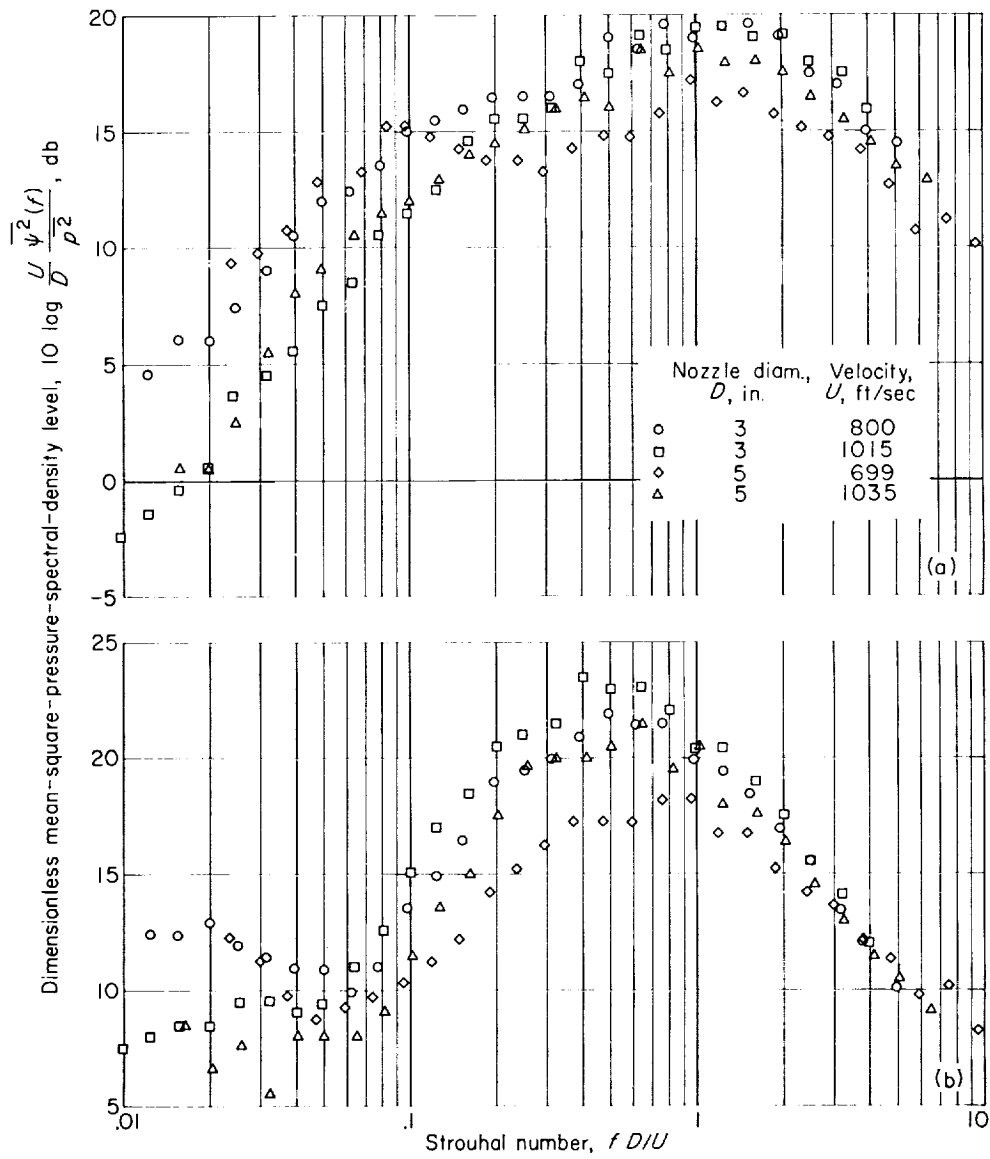
(a) $r_l = 6$ diameters; $\beta = 30°$.
(b) $r_l = 18$ diameters; $\beta = 30°$.

FIGURE 21.—Dimensionless spectra of pressure fluctuations.

Nozzle diam., D, in.	Velocity, U, ft/sec
○ 3	798
□ 3	1019
◇ 5	690
△ 5	1024
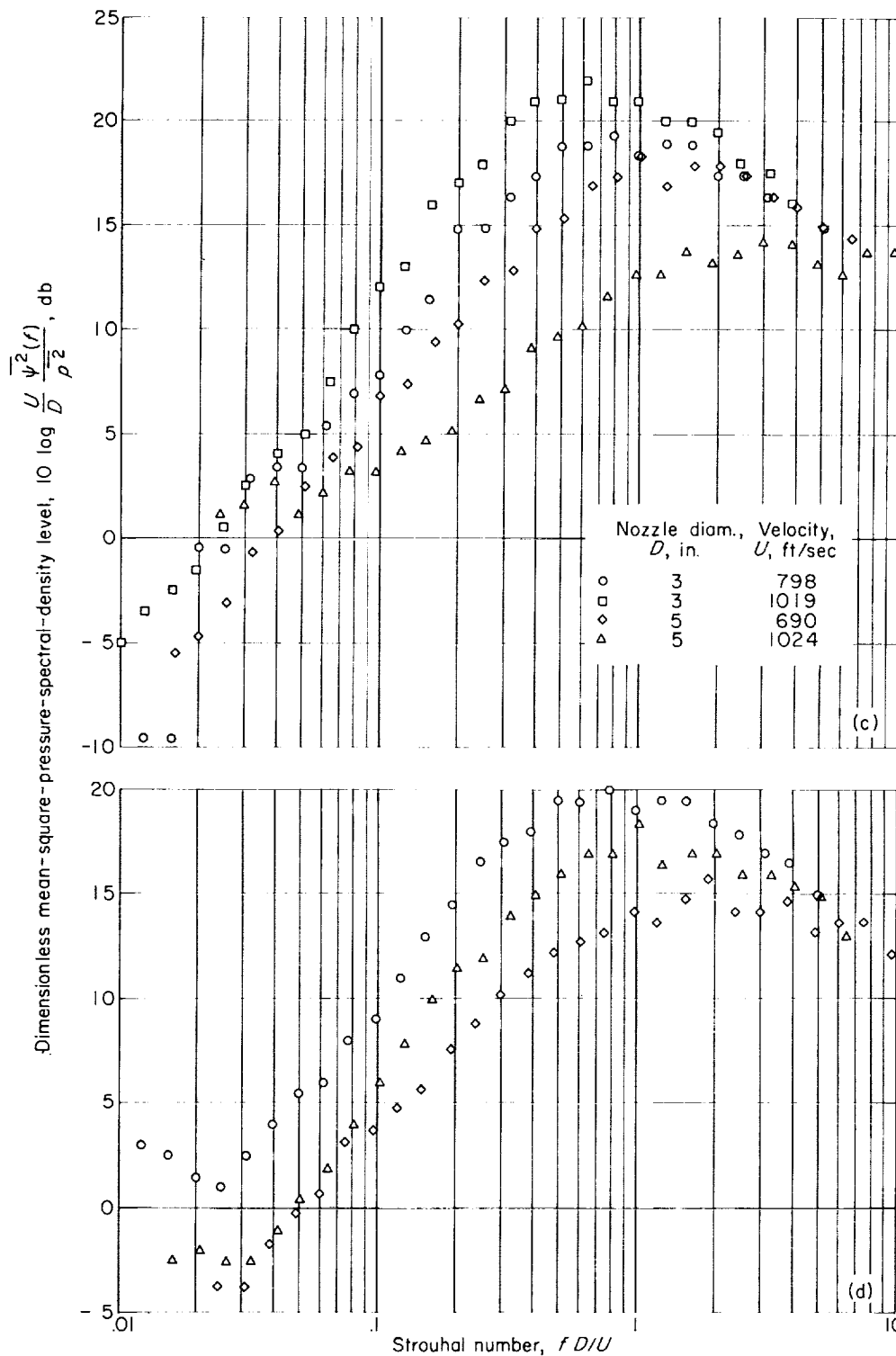
(c) $r_l = 6$ diameters; $\beta = 60°$.

(d) $r_l = 18$ diameters; $\beta = 60°$.

FIGURE 21.—Continued.   Dimensionless spectra of pressure fluctuations.

(e) $r_l=6$ diameters; $\beta=90°$.

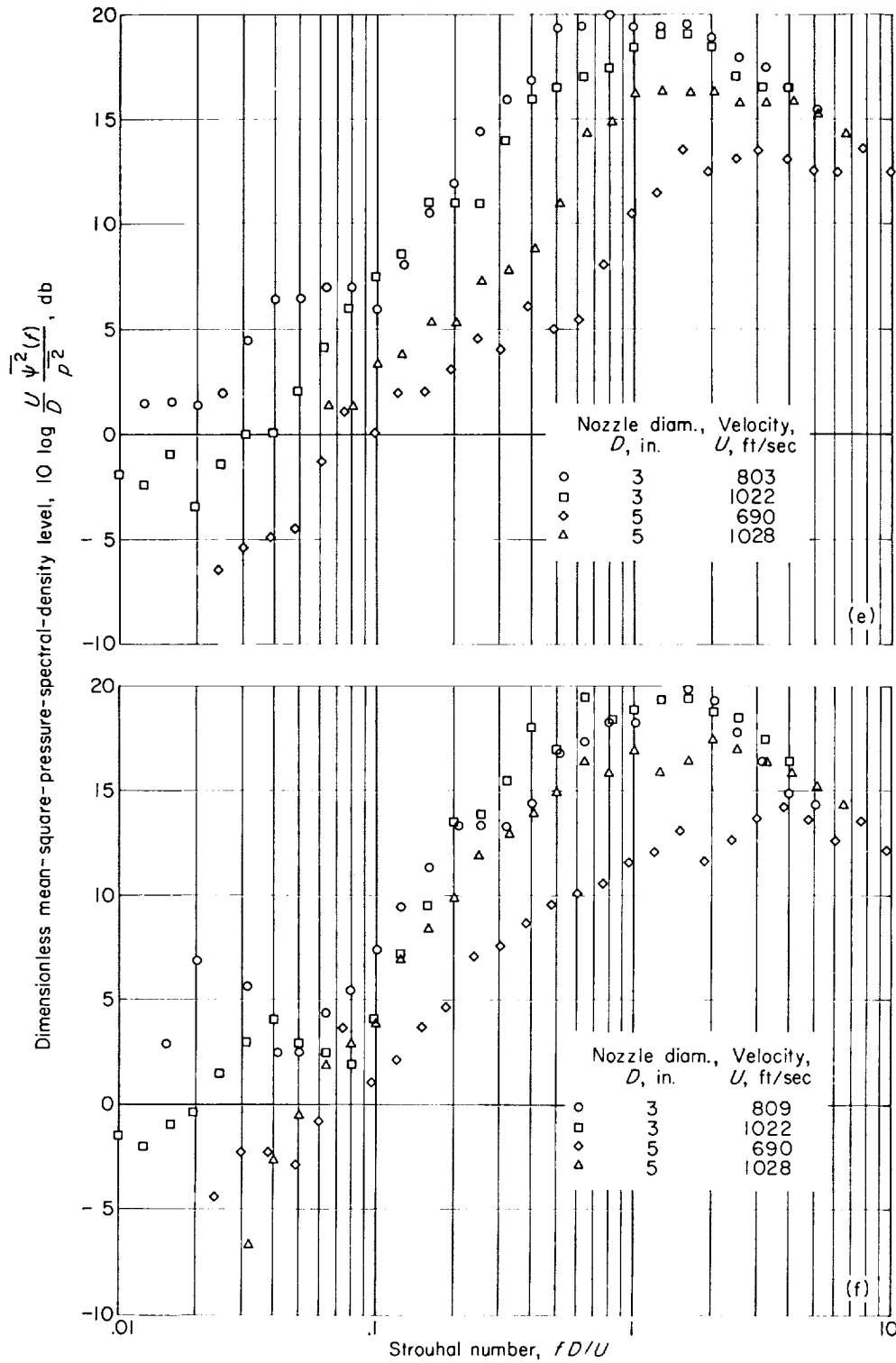(f) $r_l=18$ diameters; $\beta=90°$.

FIGURE 21.—Concluded. Dimensionless spectra of pressure fluctuations.

(a) $z^*=0$.
(b) $z^*=0.2$.

FIGURE 22.—Dimensionless fluctuation-pressure spectra along mean-velocity boundary.

(c) z^*=0.4.
(d) z^*=0.8.

FIGURE 22.—Continued. Dimensionless fluctuation-pressure spectra along mean-velocity boundary.

(e) $z^* = 1.00$.
(f) $z^* = 2.0$.

FIGURE 22.—Continued.   Dimensionless fluctuation-pressure spectra along mean-velocity boundary.

(g) $z^*=3.0$.
(h) $z^*=5.0$.

FIGURE 22.—Continued. Dimensionless fluctuation-pressure spectra along mean-velocity boundary.
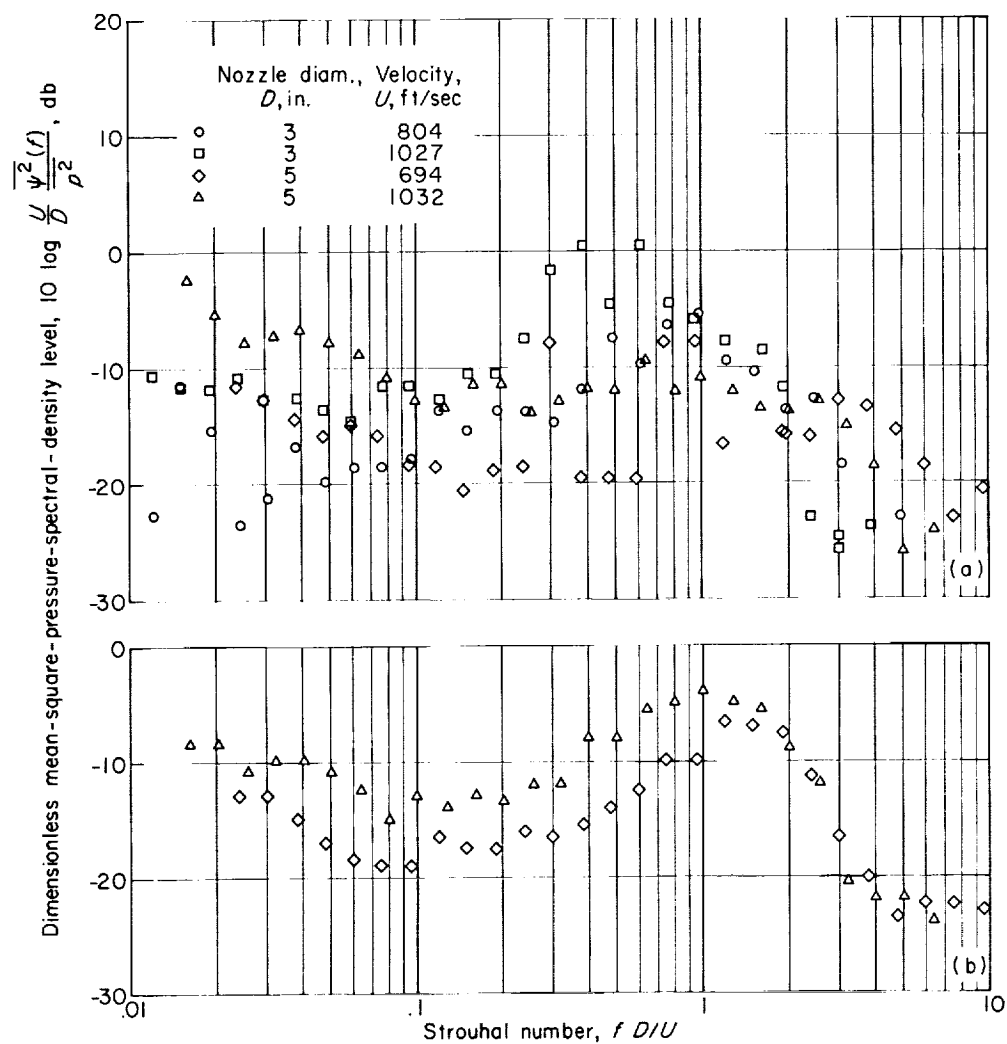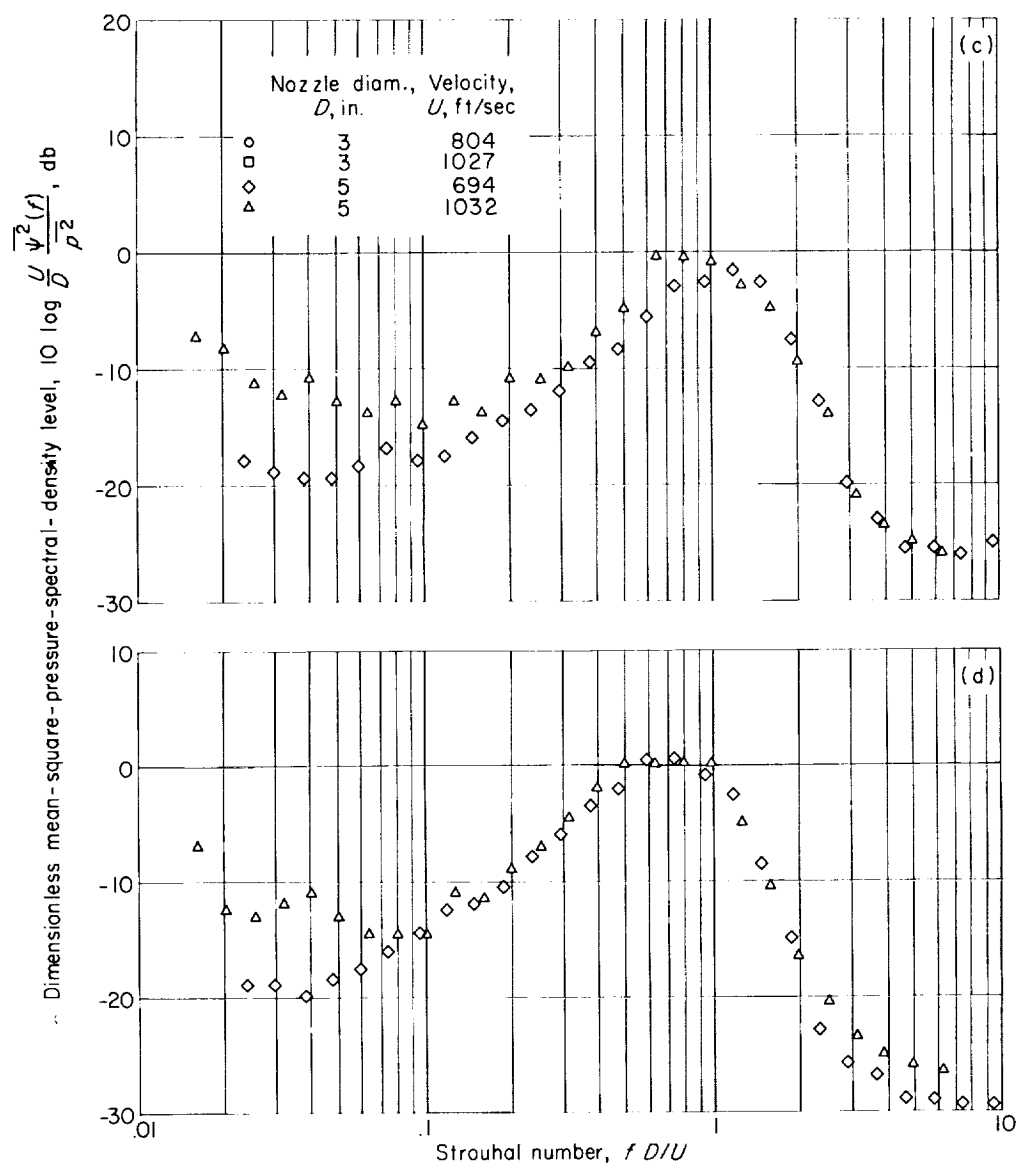
(i) $z^*=10.00$.
(j) $z^*=14.0$.

FIGURE 22.—Continued.   Dimensionless fluctuation-pressure spectra along mean-velocity boundary.

FIGURE 22.—Concluded. Dimensionless fluctuation-pressure spectra along mean-velocity boundary.
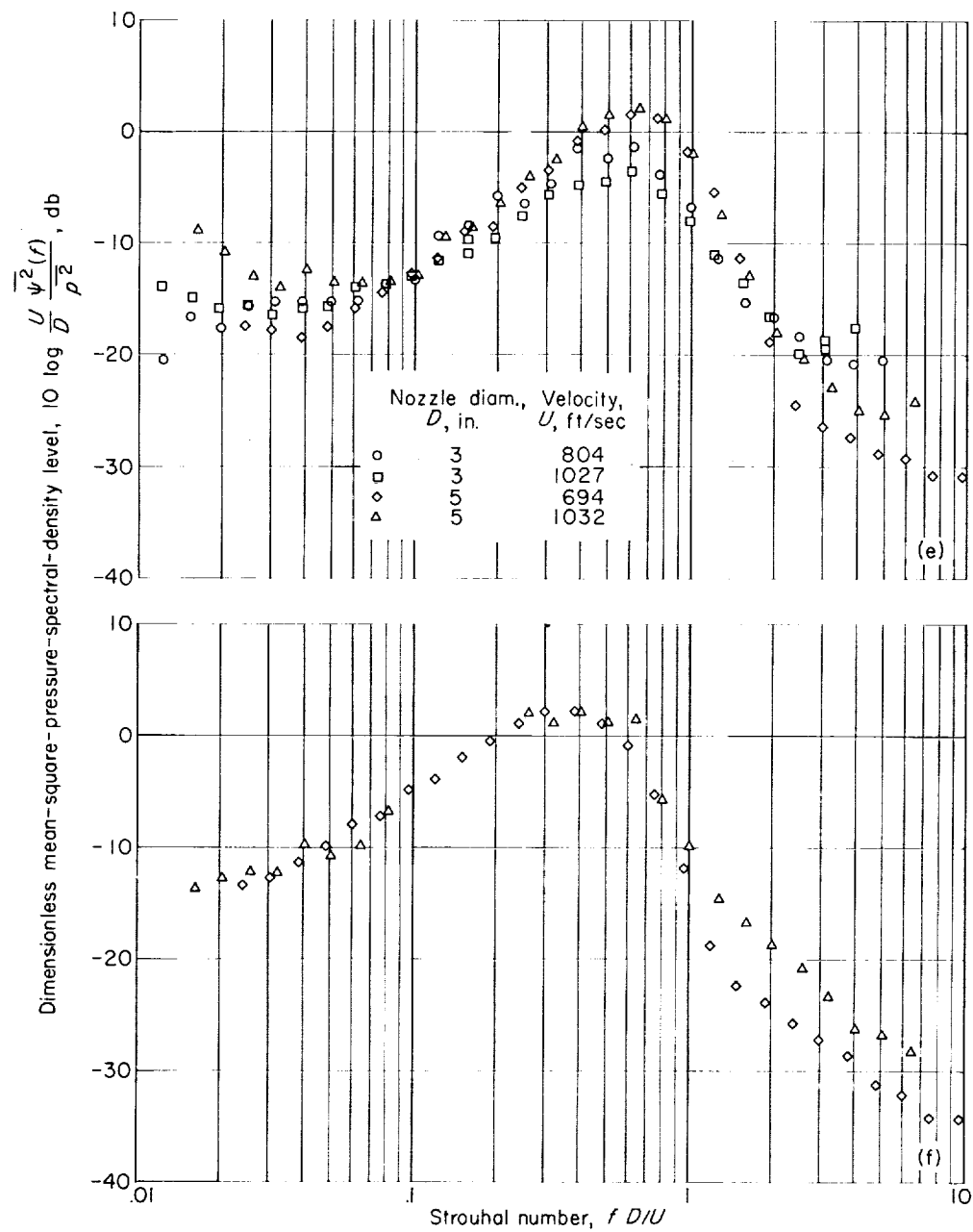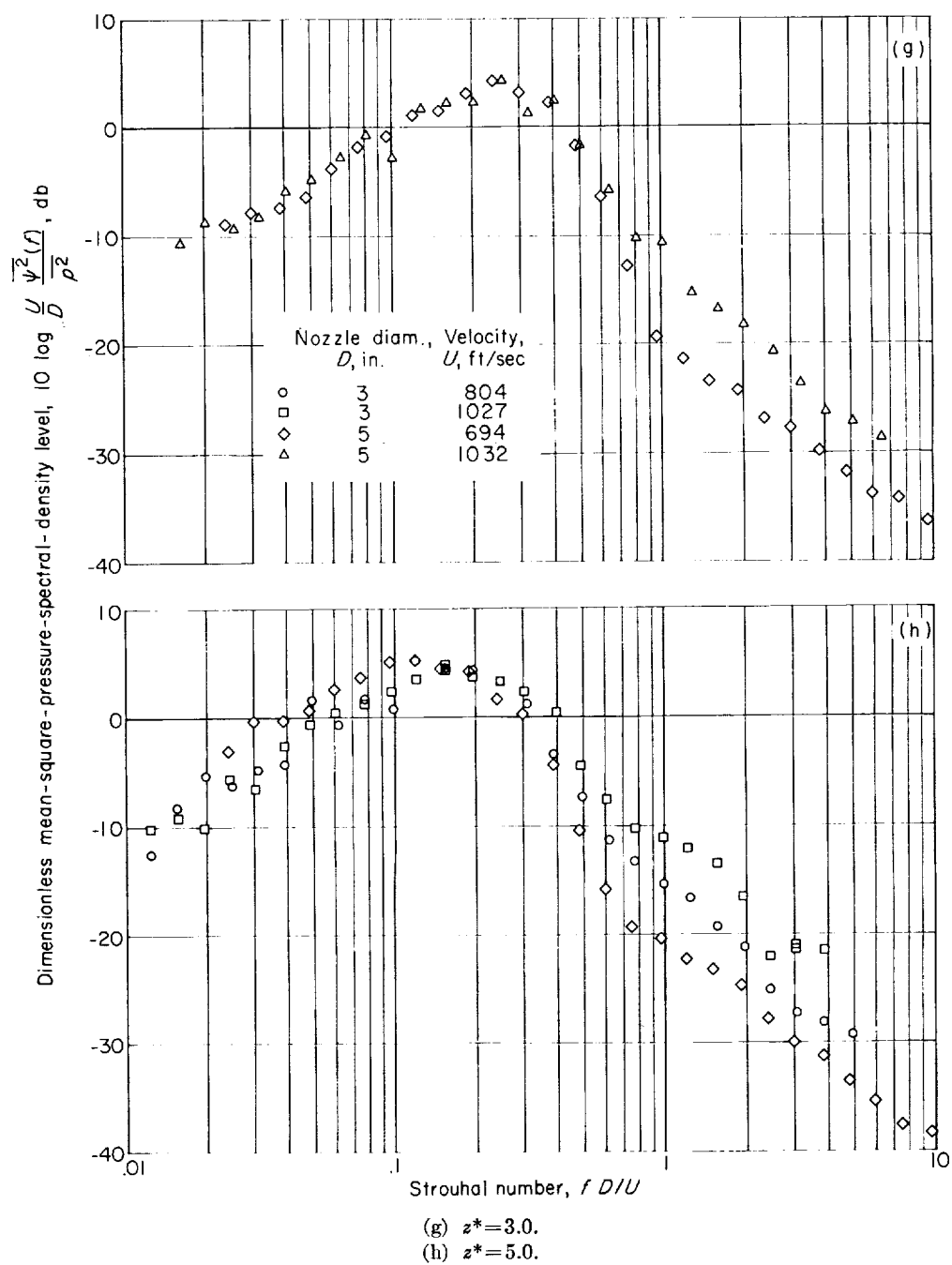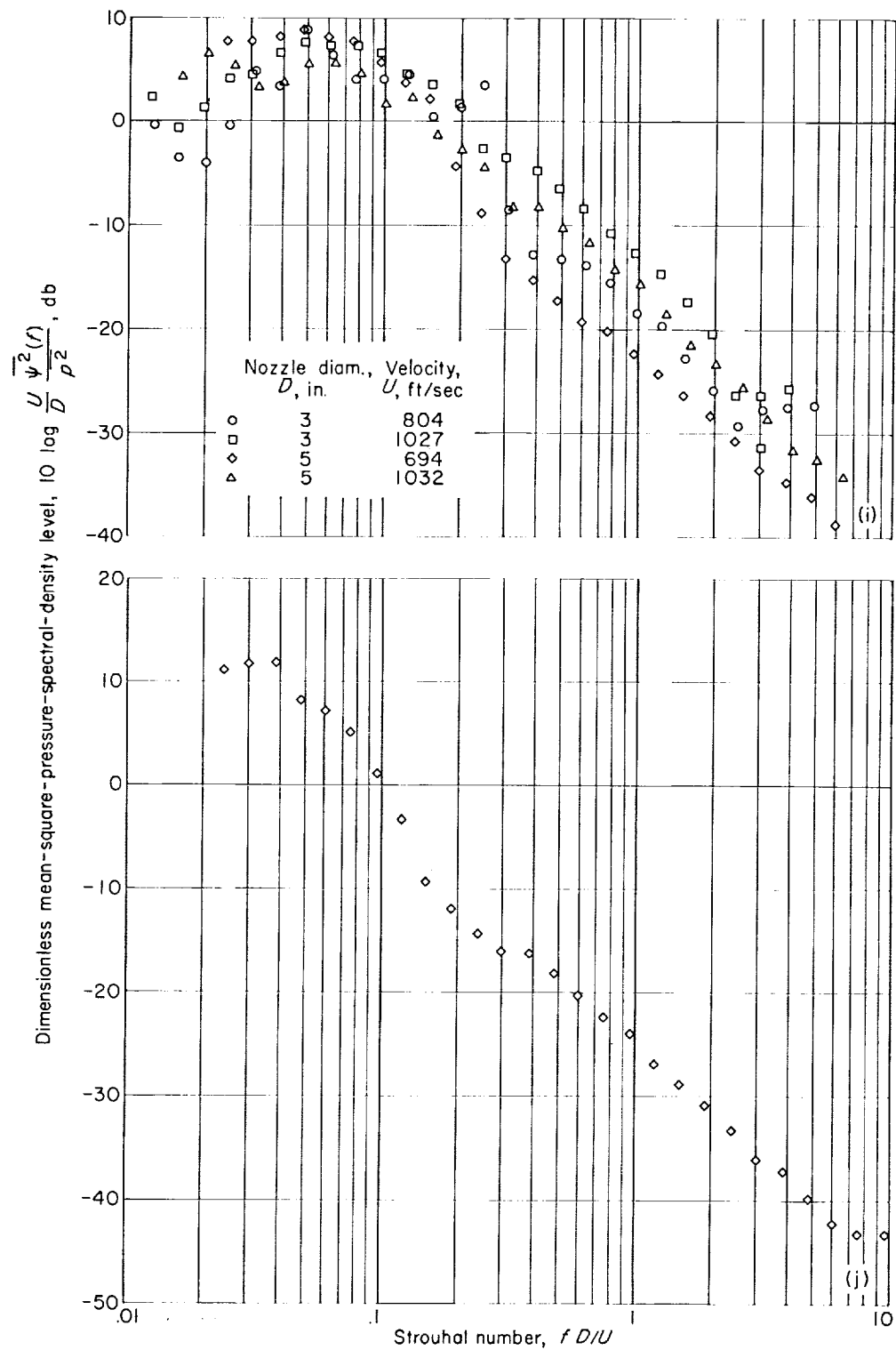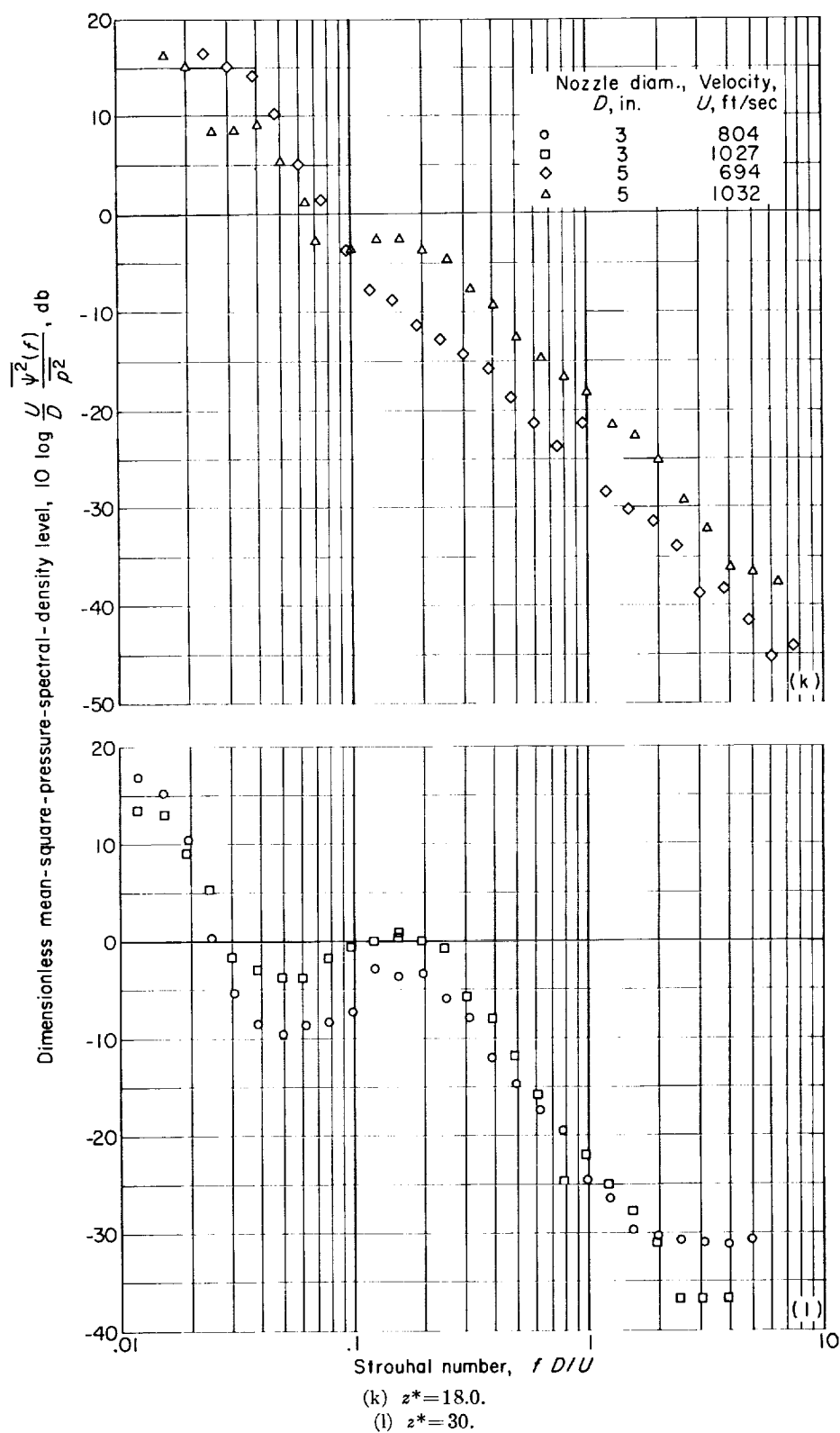
CONCLUSIONS

From a theoretical and experimental investigation of near noise fields of jets, the following conclusions were reached:

1. Similarity relations proposed by Greatrex were found to be satisfactory for predicting the characteristics of the fluctuation-pressure field for intermediate values of the flow and geometric variables if the fluctuation-pressure characteristics are known for two sets of conditions.

2. The validity of the similarity parameters, hence the predicted pressure characteristics, may be considerably reduced if nozzles having different profiles, or jets having different temperatures, are considered. This is especially true for regions near the nozzle itself.

LEWIS RESEARCH CENTER
    NATIONAL AERONAUTICS AND SPACE ADMINISTRATION
      CLEVELAND, OHIO, *August 18, 1960*

APPENDIX

SYMBOLS

a	ambient speed of sound
D	nozzle-exit diameter
F, F_1, F_2	overall-fluctuation-pressure directivity functions
f	frequency
f_a	lower cutoff frequency
f_b	upper cutoff frequency
f_m	filter geometric mean frequency, $\sqrt{f_a f_b}$
$\hat{f}$	characteristic frequency
G, G_1, G_2	spectral-density directivity functions
$k, l, m, n, \kappa, \lambda, \mu, \nu$	variable exponents
$\overline{p^2}$	mean-square fluctuation pressure for specified frequency bandwidth, overall mean-square fluctuation pressure
p_0	reference pressure (2×10^{-4} dyne/cm^2)
R	characteristic radius of observation point from effective center of noise source
r, θ, φ	spherical coordinates (see fig. 1)
r^*	r/D
r_l	radius connecting nozzle lip and observation point
r	radius in cylindrical coordinates (script lower case in figures)
r_0	radius of nozzle exit, $D/2$
r^*	r/D
SPL	sound-pressure level, $10 \log (\overline{p^2}/p_0^2)$
U	jet exit velocity
z	jet axial distance from nozzle-exit plane
z^*	z/D
α	characteristic polar angle between radius vector $\vec{R}$ and z-axis
β	field angle with origin at nozzle lip
θ^*	θ
λ	characteristic wavelength of pressure fluctuations
ν	Strouhal number, fD/U
ν_a	lower cutoff frequency in dimensionless form, $f_a D/U$
ν_b	upper cutoff frequency in dimensionless form, $f_b D/U$
ν_m	filter mean-frequency in dimensionless form, $f_m D/U$
ρ	ambient density
$\overline{\psi^2}(f)$	mean-square-pressure spectral density, $\overline{p^2} = \int_0^\infty \overline{\psi^2}(f)\, df$

REFERENCES

1. Lighthill, M. J.: On Sound Generated Aerodynamically. I—General Theory. Proc. Roy. Soc. (London), ser. A, vol. 211, no. 1107, Mar. 20, 1952, pp. 564–587.

2. Cole, J. N., et al.: Noise Radiation from Fourteen Types of Rockets in the 1000 to 130,000 Pounds Thrust Range. TR 57–354, Aero. Medical Lab., WADC, Dec. 1957.

3. Chobotov, V., and Powell, A.: On the Prediction of Acoustic Environments from Rockets. GM–TR–190, The Ramo-Wooldridge Corp., June 3, 1957.

4. Powell, Alan: Similarity Considerations of Noise Production from Turbulent Jets, Both Static and Moving. Rep. SM–23246, Douglas Aircraft Co., Inc., July 1, 1958.

5. Powell, Alan: Similarity and Turbulent Jet Noise. Jour. Acoustical Soc. Am., vol. 31, no. 6, June 1959, p. 812.

6. Powell, A.: The Generation of Noise by Turbulent Jets. Preprint 59-AV-53, ASME, 1959.

7. Howes, Walton L.: Similarity of Far Noise Fields of Jets. NASA TR R-52, 1960.

8. Ribner, H. S.: On the Strength Distribution of Noise Sources Along a Jet. UTIA Rep. 51, Univ. Toronto, Apr. 1958. (Also Jour. Acoustical Soc. Am., vol. 30, no. 9, Sept. 1958, p. 876.)

9. Lilley, G. M.: On the Noise from Air Jets. FM 2724, British ARC, Sept. 8, 1958.

10. Dyer, Ira: Distribution of Sound Sources in a Jet Stream. Bolt, Beranek and Newman, Inc., Cambridge, Mass. (See also Jour. Acoustical Soc. Am., vol. 31, no. 7, July 1959, pp. 1016–1022.)

11. Greatrex, F. B.: Jet Noise. Fifth Inter. Aero. Conf., Los Angeles (Calif.), June 1955, pp. 415–448.

12. Howes, Walton L.: Distribution of Time-Averaged Pressure Fluctuations Along the Boundary of a Round Subsonic Jet. NASA TN D-468, 1960.

13. Howes, Walton L., Callaghan, Edmund E., Coles, Willard D., and Mull, Harold R.: Near Noise Field of a Jet-Engine Exhaust. NACA Rep. 1338, 1957. (Supersedes NACA TN's 3763 and 3764.)

14. Wolfe, M. O. W.: Near Field Jet Noise. Rep. 112, NATO, AGARD, Apr./May 1957. (Also Tech. Note: Structures 228, British RAE, Sept. 1957.)

15. Franz, G. J.: The Near-Sound Field of Turbulence. Rep. 982, David W. Taylor Model Basin, Oct. 1959.

16. Townsend, A. A.: The Structure of Turbulent Shear Flow. Cambridge Univ. Press, 1956.

17. Kraichnan, Robert H.: Pressure Field Within Homogeneous Anisotropic Turbulence. Jour. Acoustical Soc. Am., vol. 28, no. 1, Jan. 1956, pp. 64–72.

18. Ribner, H. S.: New Theory of Jet Noise Generation, Directionality, and Spectra. Jour. Acoustical Soc. Am., vol. 31, no. 2, Feb. 1959, p. 245.

19. Corcos, G. M.: Some Measurements Bearing on the Principle of Operation of Jet Silencing Devices. Rep. SM-23114, Douglas Aircraft Co., Inc., Mar. 1958.